ESD-TR-76-115

Technical Report

518

R. K. Crane

Low Elevation Angle Measurement Limitations Imposed by the Troposphere: An Analysis of Scintillation Observations Made at Haystack and Millstone

18 May 1976

Prepared for the Ballistic Missile Defense Program Office,
Department of the Army,
under Electronic Systems Division Contract F19628-76-C-0002 by

Lincoln Laboratory

MASSACHUSETTS INSTITUTE OF TECHNOLOGY

LEXINGTON, MASSACHUSETTS

The work reported in this document was performed at Lincoln Laboratory, a center for research operated by Massachusetts Institute of Technology. This program is sponsored by the Ballistic Missile Defense Program Office, Department of the Army; it is supported by the Ballistic Missile Defense Advanced Technology Center under Air Force Contract F19628-76-C-0002.

This technical report has been reviewed and is approved for publication.

FOR THE COMMANDER

Raymond L. Loiselle, Lt. Col., USAF
Chief, ESD Lincoln Laboratory Project Office

MASSACHUSETTS INSTITUTE OF TECHNOLOGY

LINCOLN LABORATORY

LOW ELEVATION ANGLE MEASUREMENT LIMITATIONS IMPOSED BY THE TROPOSPHERE: AN ANALYSIS OF SCINTILLATION OBSERVATIONS MADE AT HAYSTACK AND MILLSTONE

R. K. CRANE

Group 91

TECHNICAL REPORT 518

18 MAY 1976

LEXINGTON MASSACHUSETTS

ABSTRACT

Tropospheric angle-of-arrival and amplitude scintillation measurements were made at X-band (7.3 GHz) and at UHF (0.4 GHz). The measurements were made using sources on satellites with 12-day orbits. The angle of arrival of the ray path to a satellite changed slowly allowing observations of fluctuations caused by atmospheric irregularities as they slowly drifted across the ray path. The fluctuations were characterized by the rms variations of elevation angle and the logarithm of received power (log power).

Over a one-year period, 458 hours of observation were amassed spanning every season, time of day, and weather conditions. The results show strong scintillation occurrences below 1 to 2° elevation angles characterized by a number of random occurrences of multipath events that produce deep fades, angle-of-arrival fluctuations, and depolarization of the received signal. The log power fluctuations ranged from 1 to 10 dB rms at elevation angles below 2° to less than 0.1 dB at elevation angles above 10°. The elevation angle fluctuations ranged from 1 to 100 mdeg at elevation angles below 2° to less than 5 mdeg at a 10° elevation angle. Comparable fluctuations in elevation angle are expected for bias refraction correction models based upon the use of surface values of the refractive index.

CONTENTS

LIST OF ILLUSTRATIONS

LOW ELEVATION ANGLE MEASUREMENTS IMPOSED BY THE TROPOSPHERE: AN ANALYSIS OF SCINTILLATION OBSERVATIONS MADE AT HAYSTACK AND MILLSTONE

I. INTRODUCTION

Radar systems operating within the troposphere experience measurement errors caused by spatial and temporal variations in the index of refraction. Tropospheric propagation errors occur at all elevation angles but are of major concern only at elevation angles below 5 to 10°. The Millstone Hill Radar Propagation Study[1] was undertaken to investigate the effects of the propagation medium on radar measurements. A joint Lincoln Laboratory and Bell Telephone Laboratory study was sponsored at Millstone by the U.S. Army through the Advanced Ballistic Missile Defense Agency (ABMDA) and the SAFEGUARD System Command during the February 1969 to July 1973 time period to investigate the effects of the ionosphere on radar measurement accuracy. This report describes a follow-on program conducted at the Millstone Hill Radar Facility for ABMDA to investigate the effects of the troposphere.

The gross effects of tropospheric refraction – elevation angle errors and range errors – have been studied in the past, and refraction correction models can be found in handbooks.[2,3,4] These models provide an estimate of refraction errors based upon a limited amount of data on the state of the atmosphere. The model described by Crane[4,5] was generated specifically for the Millstone Hill Radar Propagation Study. Residual refraction errors remain after the model corrections have been applied. The magnitude of these residuals depends upon the sophistication of the correction procedure and on the random fluctuations of the refraction errors that occur during an observation (or correction) period.

The residual errors are often modeled as belonging to two classes: bias errors and scintillation. The bias errors correspond to residual refraction errors that are constant or slowly varying during an observation period; scintillation corresponds to random fluctuations about the bias values. Unfortunately, a clear separation between bias effects and scintillation does not exist. Residuals that may be considered to be bias values for short observation periods may be included as scintillation for longer duration intervals. This difficulty arises from the nonstationary behavior of refraction errors: range and angle-of-arrival variances increase with increasing observation time. Additional complications occur in the estimation of bias errors due both to long-term (large-scale) variations in the atmosphere and to possible inadequacies in the correction model. Ideally, correction can be made for the bias component of the refraction error but not for the random component (scintillation). A study of refraction effects must consider both components.

To study this problem further, and to establish the limitations it imposes on the metric accuracy of a radar operating at low elevation angles, the program of propagation studies reported here was devised. In this study angle-of-arrival and amplitude scintillation were observed at 0.4 and 7.3 GHz by observing transmissions from the Interim Defense Communication Satellite Program (IDCSP) satellites. For reception, a 0.4-GHz monopulse beacon tracker at the Millstone Hill Radar Facility[6] and a 7.3-GHz beacon tracker at the Haystack Observatory, operated by the Northeast Radio Observatory Corporation (NEROC), were used. In addition, bias error residuals were observed using L-band radar sphere tracks. Radar observations were made of multiple passes of 1-, 0.2-, and 0.1-m^2 calibration spheres. Best fit orbits were constructed for each of the spheres for use as position references for observations at low elevation angles

on each of the passes. Bias error estimation requires extreme target position measurement accuracy to separate the errors caused by the instrument from the errors caused by the atmosphere. Considerable effort has been expended for the calibration of the Millstone facility.[7] Using multipass orbit fits, the position of a sphere at any instant within the time used for the orbit fit is known with an angular accuracy of better than 4 mdeg at elevation angles below 10° (an accuracy of better than 70 μrad).

L-band radar observations were made during 16 tracking sessions between 1 October 1973 and 30 September 1974 for the study of low elevation angle propagation effects. At first, most observations were of large cross section objects, but during the last four tracking sessions sphere tracks were emphasized. Coherent data recordings were also made during the last four tracking sessions to provide information on cross-section (amplitude) scintillation and phase fluctuations in addition to the position measurement data. State vectors have been generated for each of the objects tracked to provide accurate position estimates for bias error estimation. Unfortunately, due to a sudden termination of funding for this program, an analysis of the residual errors has not been performed. Except for examples of scintillation, further reference to the L-band radar data will not be made in this report.

Scintillation observations using the IDCSP satellites were made at Haystack and Millstone during 1975. Nineteen sets of measurements were made between 27 January and 11 December. The durations of the observations within a set ranged from 6 to 40 hours, and a total of 458 hours of observations was amassed during the year. The satellites were observed at elevation angles from 43° down to the horizon under all weather conditions. An extensive analysis program was planned, but due to the termination of funding only root mean square (rms) fluctuations in the logarithm of received power (log power) and angle of arrival will be reported. The rms values were calculated over 5-min. and 1-hr intervals about quadratic curves fitted by least squares to the data within an observation interval to remove the mean trend. No attempt has been made to study the angle bias errors: only scintillation is considered in this report.

Observations were made simultaneously at 0.4 and 7.3 GHz. The antennas used for these observations are separated by a distance of 0.7 km, i.e., significantly larger than the correlation distance for amplitude fluctuations at either frequency. The simultaneous observations are not useful for studying the correlation between the fluctuations at both frequencies but are useful for examining the frequency dependence of the rms fluctuation values.

Crane[8,9,10] has reported a theoretical analysis and observations of the frequency dependence of rms fluctuations in the logarithm of received power (log power), doppler, and angle of arrival caused by ionospheric scintillation. The same weak scintillation theory (Rytov approximation) is valid for tropospheric scintillation when the results given in Refs. 8, 9, and 10 are modified to account for the differences in wavelength dependence between ionospheric and tropospheric indices of refraction. Weak scintillation theory coupled with an assumed $\kappa^{-11/3}$ three-dimensional (3-d) power spectral density for tropospheric refractivity fluctuations (κ = wavenumber yields an estimated $\lambda^{-7/12}$ wavelength dependence for rms variations in log power (σ_χ). The wavelength dependence for angle-of-arrival and Doppler fluctuations is given by λ^0 and λ^{-1}, respectively. The last results do not depend upon the exponent of the assumed refractive index spectrum. The Haystack and Millstone observations are in agreement with the predicted wavelength dependence for σ_χ for measurements at low elevation angles.

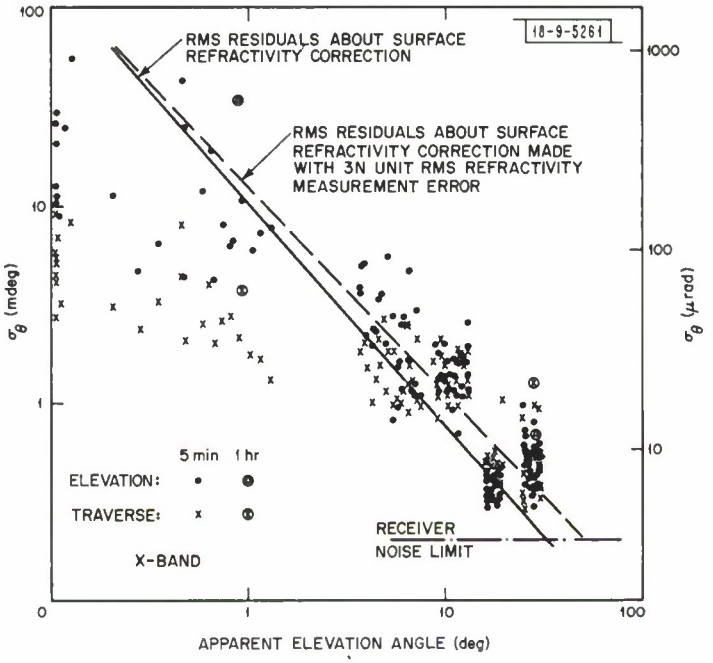

Fig. I-1. Elevation and traverse angle fluctuations; 13-15 September 1975; weather, cloudy.

The angle-of-arrival observations show the expected increase in the rms value with increasing observation time. Figure I-1 displays the observed rms fluctuations in elevation and traverse [azimuth × cos (elevation)] for one of the observation sets made under conditions of fair-weather cumulus clouds and clear sky. These data show rms errors of less than 50 μrad for elevation angles above 10°. Figure I-1 also displays the expected rms residual errors about the surface refractivity model for estimating bias errors generated for Millstone.[5] The observed scintillations are within a factor of two of the expected fluctuations in bias error estimation. The results displayed on Fig. I-1 are typical of those obtained on each observation set suggesting that the surface correction model represents a practical limit for refraction correction. Bias error correction estimates are expected to apply for periods of an hour or more, and because the rms fluctuations due to the natural variability of the atmosphere exceed those expected from ray tracing analysis for the surface correction model, better bias estimates are not warranted.

This report describes the X-band instrumentation used at Haystack, the changes in the UHF instrumentation from the configuration reported by Ghiloni,[6] and the processing programs. Sample observations and rms fluctuation data are presented in Section III. A comparison between observations and the predictions of weak scintillation theory is given in Section IV. Conclusions are presented in Section V.

II. INSTRUMENTATION

A. Haystack

The goal of the measurement program at Haystack was to observe angle and amplitude scintillation over the widest possible range of elevation angles. Information on elevation angle dependence was required to define the minimum useful elevation angle for achieving a specified angular measurement precision (rms error). Observations at elevation angles above 5° were also desired for modeling amplitude scintillation at higher frequencies. Earlier observations had shown that the rms fluctuations in log power (σ_χ) should be less than 0.2 dB and rms fluctuations in angle of arrival (σ_θ) should be less than 2 mdeg for elevation angles above 5° (Ref. 11). To make observations at higher elevation angles, design goals were set to obtain measurements with instrumental noise contributions of less than 0.05 dB rms in log power and 0.4 mdeg rms in angle of arrival. To achieve these goals using Haystack and the IDCSP 7299.5-MHz beacons, a very narrow bandwidth monopulse tracking receiver system was designed. Computer-aided automatic angle and frequency tracking was used to keep the antenna pointed within 4 mdeg of the apparent position of the source and to tune the receiver to track within 0.5 Hz of the apparent frequency of the source. This precision was required to maintain less than 0.1-dB variations due to the instrument in received signal level.

The 36.6-m (120-ft) Haystack antenna[12,13] was fitted with a conventional 4-horn monopulse feed. Four identical receiver channels were provided: principal polarization (left-hand circular) sum (ΣLH), principal polarization elevation difference (ΔEL), principal polarization traverse difference (ΔAZ), and orthogonal polarization sum (ΣRH). The receiver channels are schematically described in Fig. II-1. Quadrature video was provided to the A/D converters after four stages of frequency conversion and IF amplification. First-stage mixer amplifiers with an 8-dB noise figure were mounted behind the tracking feed in the radiometer box.[12] Doppler corrections obtained from orbital calculations were provided at the second IF stage. Manual frequency control was provided at the third stage to compensate for the long-term drift of the oscillators on the IDCSP satellites. The frequency tracking loop was closed through the CDC-3300 computer at the fourth stage.

The phase of the 2-MHz local oscillator reference signal was advanced 90° every fifth A/D sample. This interchanged the role of the two phase detectors and provided a means to compensate for DC offsets and nonorthogonality between the sine and cosine components of the quadrature video. The quadrature signals were sampled at a 200-Hz rate. Coherent computer processing of 20 successive data samples synchronized with the 90° phase advance of the local oscillator was performed to synthesize the final 10-Hz predetection filter.

The computer-aided autotrack system is depicted in Fig. II-2. The U490 computer provided the initial pointing commands as well as the Doppler corrections using orbital ephemeris data. Elevation and azimuth error data obtained from the difference channels were smoothed and used to generate differential pointing commands (demand offset). The sum of the U490 calculated position and the demand offset was used to position the antenna. Antenna position data (19-bit encoder values) were sampled by the CDC-3300 computer for use in post-test analysis. The elevation and azimuth error signals in phase with the principal polarization sum signal were normalized and used to generate the differential pointing commands (demand offset). The complex error signals together with the complex sum channel signals, time, and antenna position encoder values were recorded at a 10 sample per second rate for post processing. The angle

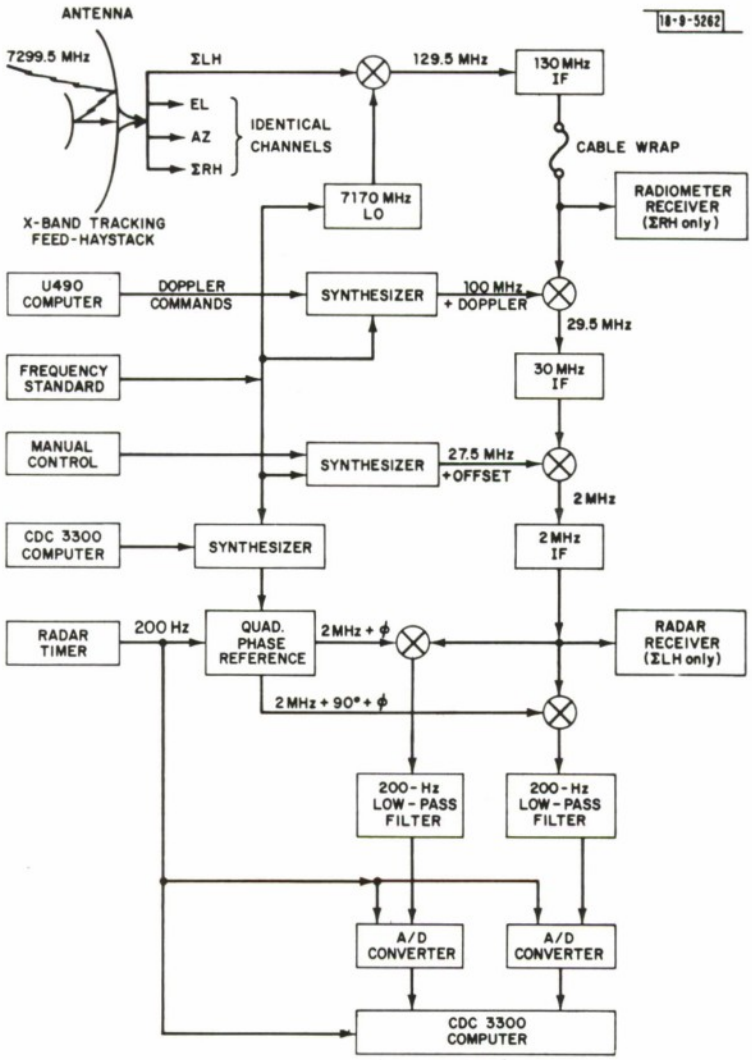

Fig. II-1. X-band receiver system.

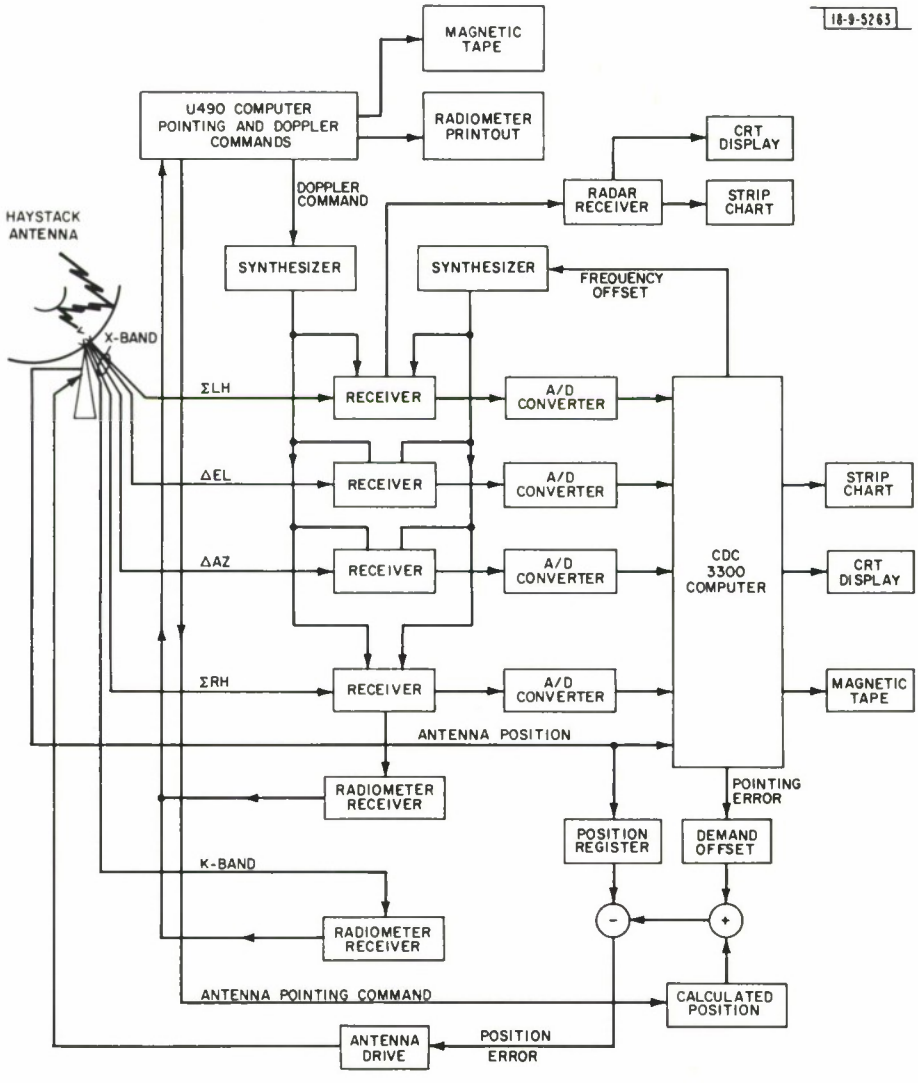

Fig. II-2. X-band tracker.

encoder values were sampled at the 200-Hz rate and averaged prior to recording and to generating the pointing commands.

The recorded complex signal data were detected, averaged, and used to generate scintillation statistics in a subsequent analysis program. Using this tracking system and 10-sample post-detection averaging, the signal-to-noise-ratio for the IDCSP satellites ranged from 40 to 45 dB. The corresponding minimum detectable rms fluctuations in log power due to receiver noise ranged between 0.04 and 0.06 dB. The signal-to-noise ratio varied within this range due to differences between the eight IDCSP satellites that were still operating during the 1975 season, due to changes in signal level caused by variations in the distance between the satellite and receiver station and in the amount of atmospheric absorption at low elevation angles as the satellite rose or set, and as a result of transponder usage on the satellites. However, only one instance of signal level change due to transponder use was noted during the observations. The receiver noise limitations on angle measurement[2] ranged from 0.2 to 0.4 mdeg rms. The X-band receiver system plus 10-sample post-detection processing achieved the desired measurement precision.

Radiometer receivers available at the Haystack Observatory were used with the X-band system to provide additional information about the atmosphere along the observation path. A 20-MHz total power X-band radiometer was used with the orthogonal polarization sum channel. This radiometer was available for use on any channel by cable changes, and was used to observe the bright radio stars Cassiopeia A and Cygnus for antenna pointing calibration. The monopulse feed was mounted off axis in the elevation plane. The pointing corrections obtained from the radio star observations were $-0.075 \pm 0.005°$ in elevation and $+0.005 \pm 0.005°$ in traverse. These offsets were added to the reported encoder position values prior to analysis. A 15-GHz, 500-MHz-bandwidth Dicke switched radiometer was also used during the measurement program. The feed for this radiometer system was on axis and no pointing correction was required.

B. Millstone

The UHF beacon tracker at Millstone was used to track the 401-MHz telemetry signal transmitted by the IDCSP satellites. Because the satellites are no longer in active use, the telemetry signal was stable in amplitude and provided an adequate source for scintillation observations. The receiver system was used as configured for the earlier Millstone Radar Propagation Study.[6] Data obtained from the receiver were sampled at a 10-Hz rate and transferred to the CDC-3300 computer at Haystack via the Millstone/Haystack intersite link. At first, only the AGC level was sampled and recorded. As the experiment progressed, the data transfer system was modified to provide complex difference channel signals, complex orthogonal polarization signal, and the Millstone antenna encoder values. The IDCSP transmission at UHF had highly elliptical polarizations. Nearly equal amplitude signals were available on the principal (right-hand circular) and orthogonal polarization channels. The elevation and traverse difference channels were right-hand circular polarization.

III. OBSERVATIONS

A. Amplitude Fluctuations

The IDCSP satellites were tracked as they rose or set. The satellites were in near-synchronous orbits moving slowly with respect to a ground station. The orbital period for each satellite was approximately 12 days with each satellite visible for about 5 days. At Haystack, the apparent angular motion was typically only two beamwidths in five minutes. At this slow angle tracking rate, the satellite-to-ground station geometry was essentially fixed while the atmosphere drifted across the path.

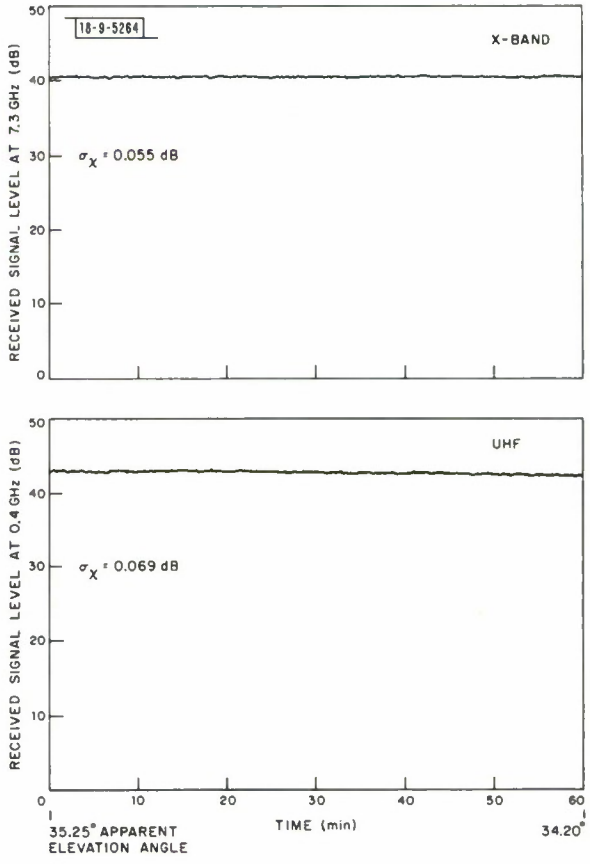

Fig. III-1. Received signal levels at high elevation angles.

Examples of observed received signal level fluctuations are given in Figs. III-1 and -2 for high and low elevation angles, respectively. The high-angle data are for elevation angles between 35.25 and 34.20° and display fluctuations near the thermal noise limit. For this satellite, at X-band (7.3 GHz) the signal-to-noise ratio was 42 dB in a 1-Hz band; at UHF (0.4 GHz) the signal-to-noise ratio was 39 dB in a 1-Hz band. The measured rms fluctuations at X-band were slightly higher than the values expected due to thermal noise because of small additional fluctuations caused by satellite spin; the satellites were spinning at 150 rpm, and 0.1 to 0.2 dB peak-to-peak modulation at the spin rate was usually evident. The combined effect of spin and thermal noise increased the X-band received signal level fluctuations to the 0.06-dB level. Slight changes in the minimum detectable σ_χ value were observed but the minimum value never exceeded 0.07 dB.

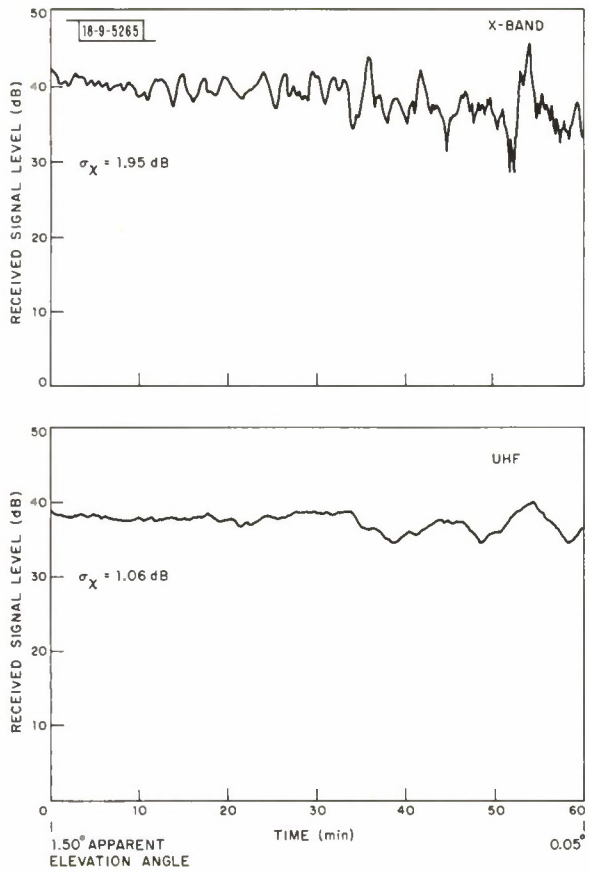

Fig. III-2. Received signal levels at low elevation angles.

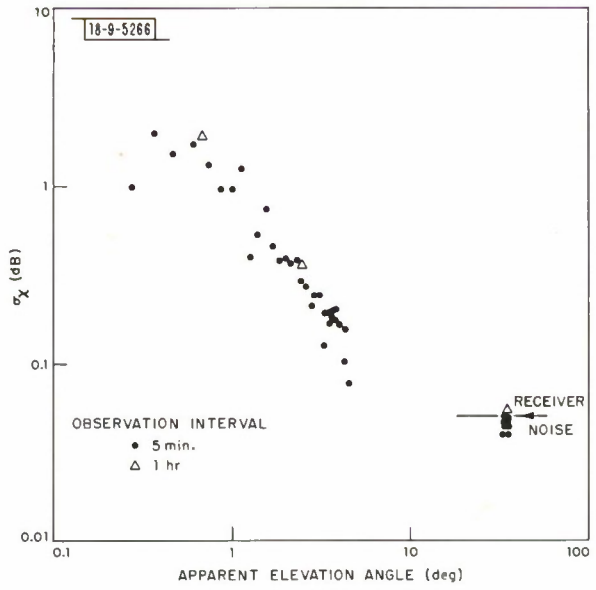

Fig. III-3. RMS fluctuations in log power at X-band.

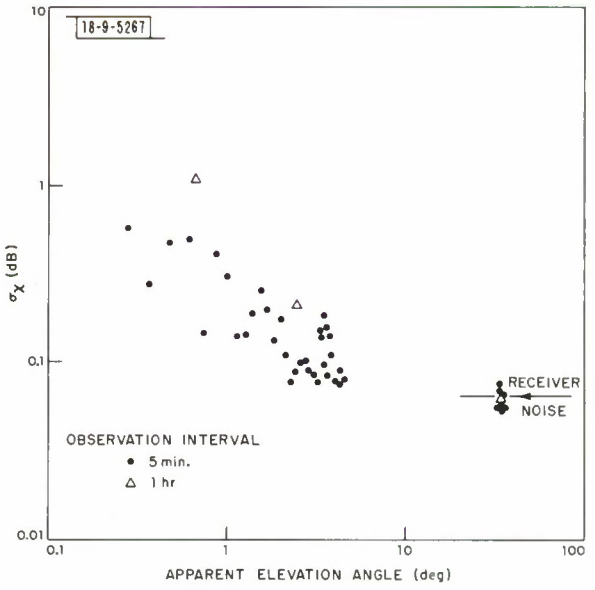

Fig. III-4. RMS fluctuations in log power at UHF.

The signal-to-noise ratio for the UHF (0.4-GHz) observations was slightly lower, and the combined effect of satellite rotation and thermal noise limited the principal polarization channel (right-hand circular) σ_χ values to a minimum of 0.07 dB. The principal polarization channel output was reconstructed from an automatic gain control (AGC) voltage with an effective 10-Hz predetection bandwidth. Orthogonal polarization measurements at UHF were made with a coherent receiver phase locked to the principal channel receiver. The predetection bandwidth for the quadrature signals was 250 Hz for most of the observation sets and 10 Hz for measurements made in November and December. With the 10-Hz filters, the σ_χ values for the orthogonal channel had a minimum of 0.07 dB. The minimum values for the principal and orthogonal channels varied slightly as the transmitted polarization changed.

The signal level fluctuations increased significantly at low elevation angles. Figure III-2 depicts the 1-sec-averaged X-band and UHF data for elevation angles between 1.5 and 0°. The horizon was at − 0.22° in the direction of set, and the satellite was tracked for an additional 10 min. before disappearing below the radio horizon. For the 73-mdeg beam of the Haystack antenna, the effect of ground multipath and horizon diffraction is negligible for the data in this figure, i.e., the fluctuations depicted in Fig. III-2 are entirely caused by the lower atmosphere. At UHF, the antenna beamwidth is 2.5° and the fluctuations between 20 and 60 min. (time) are primarily due to interfering reflections from the ground. The fluctuations at X-band appear to have a quasi-periodic behavior. At UHF much smaller fluctuations with a roughly similar temporal behavior appear to ride the longer duration fluctuations caused by the ground.

The rms values given on each of the figures are calculated rms fluctuations (in dB) about the mean trend. These rms values were calculated for each hour of data, with the start of the one-hour interval occurring on the hour. The rms fluctuations were calculated relative to a quadratic curve least square fit to the data over that hour. The quadratic curve was used to remove slow changes in signal level caused by the changes in satellite-to-ground station geometry and atmospheric absorption. RMS values were also calculated for successive 5-min. intervals occurring within the hour. A similar curve fitting procedure was also used for the 5-min. intervals. The fluctuations observed over 5-min. intervals were expected to represent uncertainty that would be associated with a single fixed observing geometry (no change in elevation angle).

Examples of the 5-min. and 1-hr rms fluctuation values for the data given in Figs. III-1 and -2 and observations made within 12 hours of each of these data sets are given in Figs. III-3 and -4. The data are for 3 IDCSP satellites, viz, one "rise" observation spanning 3 to 4° elevation (El) at 260° azimuth (Az), one "set" observation spanning 5° to 0° El at 100° Az, and a high-elevation observation spanning 37 to 33° El at 190° Az. The data were obtained between 0900 and 2100 UT 1 December 1975. The 1-hr σ_χ values for Figs. III-1 and -2 and an additional 1-hr time period within the data set are shown in these figures. The quasi-periodic fluctuations shown on Fig. III-2 have 2- to 4-min. periods while the ground reflection effects at UHF have much longer period fluctuations. The detrending (curve-fitting) process used to generate the 5-min. rms values removes most of the variance due to the long-period fluctuations evident in the 1-hr sample. This causes a difference between the 5-min. and 1-hr variance values, which is largest for the UHF data.

B. Elevation Angle Fluctuations

Angle-of-arrival estimates were produced for each of the ten/second data samples by combining the recorded averaged encoder values and averaged inphase error voltages. A

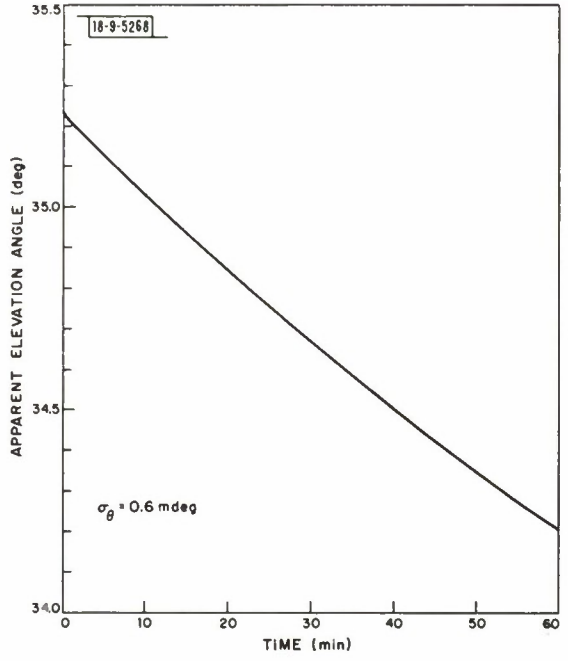

Fig. III-5. Apparent elevation angle at X-band, high-angle data.

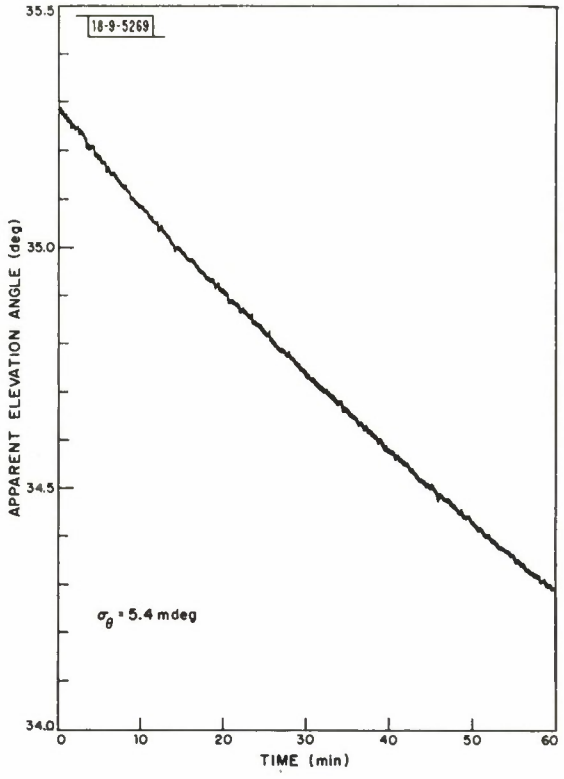

Fig. III-6. Apparent elevation angle at UHF, high-angle data.

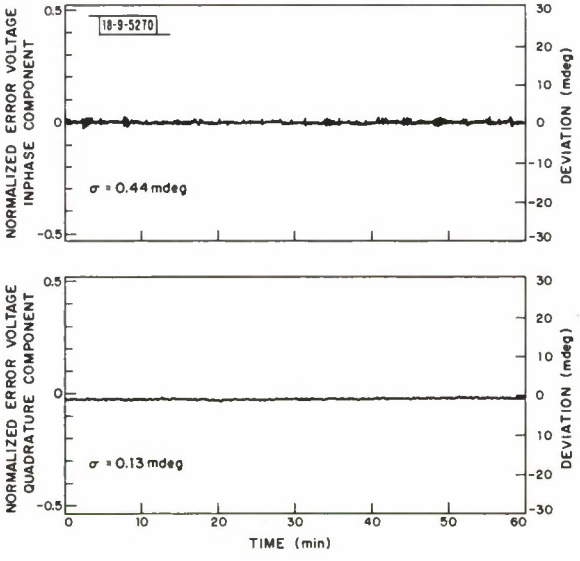

Fig. III-7. Normalized elevation angle error voltages, high-angle data.

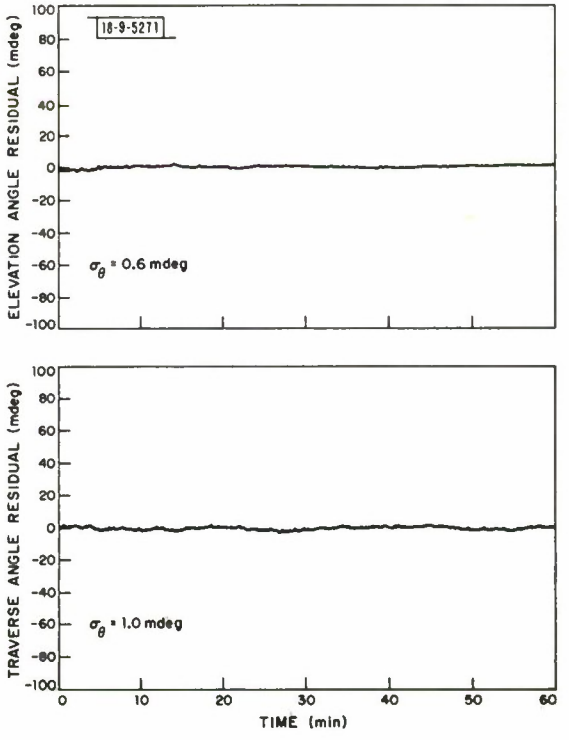

Fig. III-8. Elevation and traverse angle residuals, high-angle data.

predetermined calibration constant was used to convert the normalized error voltage (error channel voltage inphase with the sum channel signal divided by the magnitude of the sum channel voltage) into an angle deviation relative to the position encoder value. Error voltage-to-angle calibration curves were obtained occasionally at X-band and during each observation set at UHF. (The calibration constants and phases of the difference channels relative to the sum channel were very stable at X-band. The calibration constants had to be modified only once during the observation program after the waveguide connections to the X-band feed were disturbed.) The UHF system was manually adjusted prior to each set of observations, and new calibration curves were required for each data set. Unfortunately, the calibration curves could only be determined *after* initial data processing and, at the current level of data reduction, the available UHF angle-of-arrival values had to be generated using a nominal rather than the correct calibration curves.

Elevation angle estimates averaged over one second are depicted for the high elevation angle observations (Fig. III-1) in Figs. III-5 and -6. The signal level fluctuations were near the receiver noise limit. For the 73-mdeg Haystack beam and the 42-dB signal-to-noise ratio achieved in a 1-Hz band, the theoretical angle measurement limit is 0.3 mdeg (Ref. 2). The angle encoder system at Haystack suffered one to two 5- to 10-mdeg random errors or "glitches" within each tenth of a second sampling interval due to an encoder system malfunction. Efforts to remedy this defect by detecting the improper reported positions in the computer proved difficult, and for data reported here the encoder readings taken at 200 values per second were averaged to reduce the effect of these "glitches." The net effect of the "glitches" was to cause an additional rms fluctuation of less than 0.3 mdeg. The combined expected rms measurement error is less than 0.4 mdeg. The observed 1-hr rms measurement error was 0.6 mdeg. The difference between the expected and observed rms errors is due to the curve fitting procedure used to detrend the data (estimate biases). The theoretical angle-of-arrival measurement limitation due to receiver noise was 20 mdeg for the 2.5° Millstone beam. The theoretical estimate is based upon a 39-dB signal-to-noise ratio and a 1-Hz bandwidth. Due to the requirement of using only a nominal error voltage-to-angle calibration curve, the error voltage contribution to the angle-of-arrival fluctuation was significantly underestimated for the data presented in Fig. III-6. The autotrack system has a time constant larger than 1 sec, causing the observed rms fluctuation value to be less than the theoretically predicted value.

The X-band inphase and quadrature elevation angle error voltages and corresponding angular deviations are displayed in Fig. III-7. The closed-loop computer-aided tracker had a 7-sec time constant. The inphase error voltage was used to control the antenna position, and the observed fluctuations were in part caused by tracker system oscillation. The quadrature error data are also displayed in the figure. These data were not used in real time for tracking. A small non-zero quadrature error voltage is apparent in these data. The quadrature voltages generally exhibited small non-zero long-period fluctuations that depended upon the polarization of the satellite transmission.

The residual elevation angle errors that remained after curve fitting to one hour of data are shown in Fig. III-8. The tracker oscillation is not evident in these data since the use of both angle encoder data and error voltage data in constructing angle-of-arrival estimates removes any antenna positioning uncertainties. The residual error data show slow deviations from the quadratic curve which are caused by using only a second-order equation to represent the bias errors. Traverse angle residual errors are also displayed in Fig. III-8.

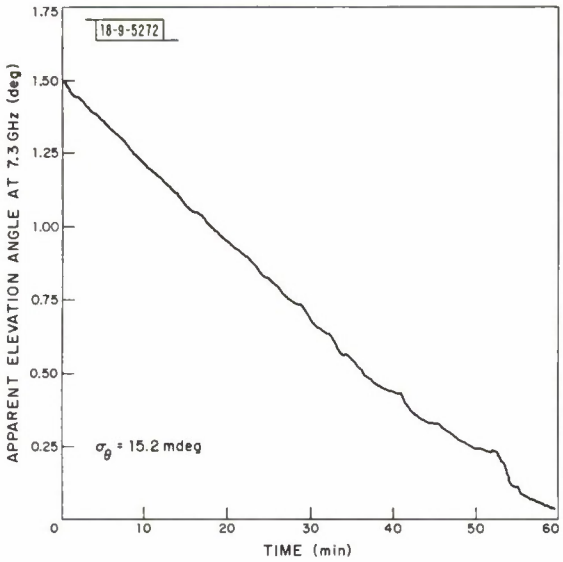

Fig. III-9. Apparent elevation angle at X-band, low-angle data.

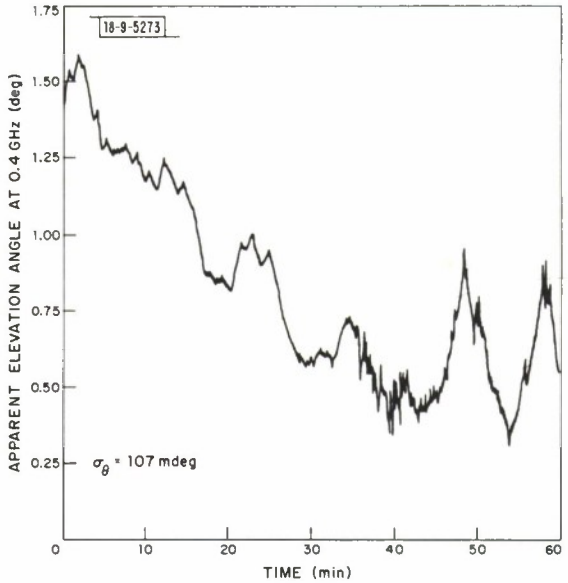

Fig. III-10. Apparent elevation angle at UHF, low-angle data.

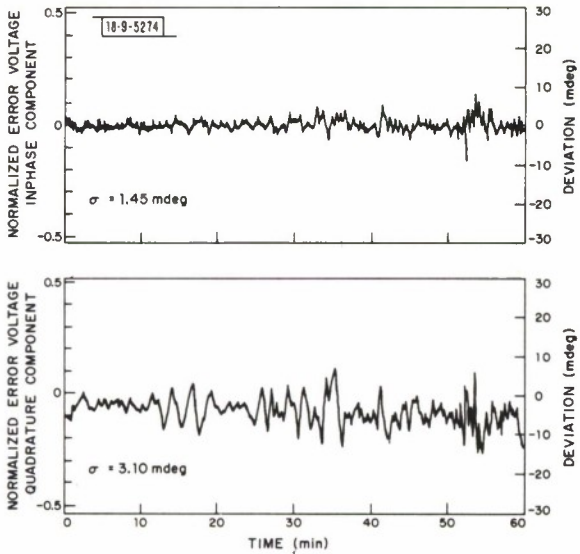

Fig. III-11. Normalized elevation angle error voltages, low-angle data.

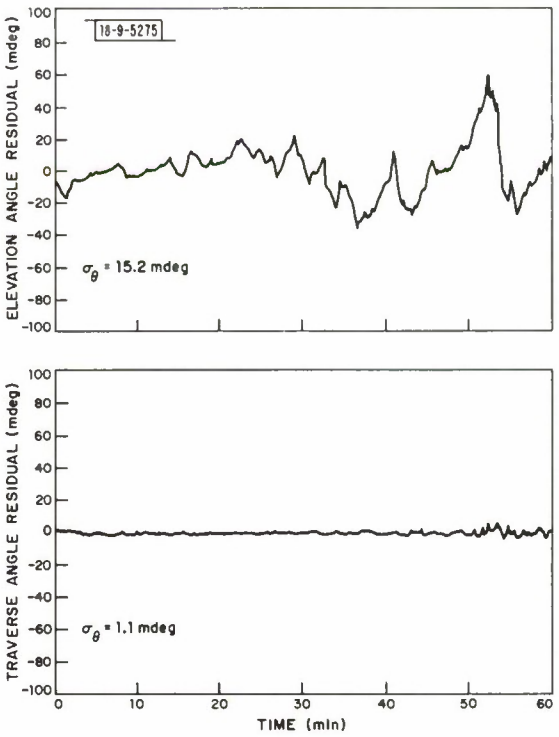

Fig. III-12. Elevation and traverse angle residuals, low-angle data.

At low elevation angles, fluctuations due to the atmosphere were evident at X-band as shown in Fig. III-9 and fluctuations due to the ground were evident at UHF as shown in Fig. III-10. The X-band inphase and quadrature error voltages are displayed in Fig. III-11, and the X-band elevation and traverse angle residuals are displayed in Fig. III-12. These observations reveal elevation angle fluctuations that are significantly greater than the noise, "glitch," and curve fitting errors displayed in Fig. III-8. The elevation angle residuals increase as the elevation angle decreases; the traverse angle residuals appear to exceed measurement noise for only the last 10 min. or for elevation angles below 0.25°. The X-band observations are at angles sufficiently high above the horizon to exclude ground reflection effects. The inphase angle deviations (Fig. III-11) are all less than 10 mdeg. Although at times the angle deviations exceed 4 mdeg, the signal level fluctuations are far larger than can be attributed to antenna gain changes caused by the apparent angle-of-arrival deviation. These observations show that the X-band system successfully maintained track during severe scintillation and that any signal level changes that may have occurred due to angle-of-arrival deviations were negligible.

The quadrature component of the normalized error voltage shows relatively large quasi-periodic fluctuations that are similar to the received signal level fluctuations displayed in Fig. III-2. A close comparison between the two curves shows that the quasi-periodic fluctuations are displaced by a quarter of a period as shown in Fig. III-13. Both UHF and X-band data are displayed in Fig. III-13, and both show this apparent quarter-period displacement between the received signal and quadrature error curves. This relationship is characteristic of a complex monopulse receiver system response to multipath.[14] At X-band the characteristic complex monopulse system response is evident in the figure for times between 10 and 20 min. The peak-to-peak signal level change is 4 dB. Two signals with a 12-dB difference in level can combine to produce this effect. Since the elevation angle for this multipath event is close to 1°, i.e., more than 16 beamwidths above the horizon, and the antenna gain in the direction of the horizon is more than 40 dB below the mainlobe peak, the multipath signal could not have originated from a ground reflection but must have been generated within the atmosphere. At

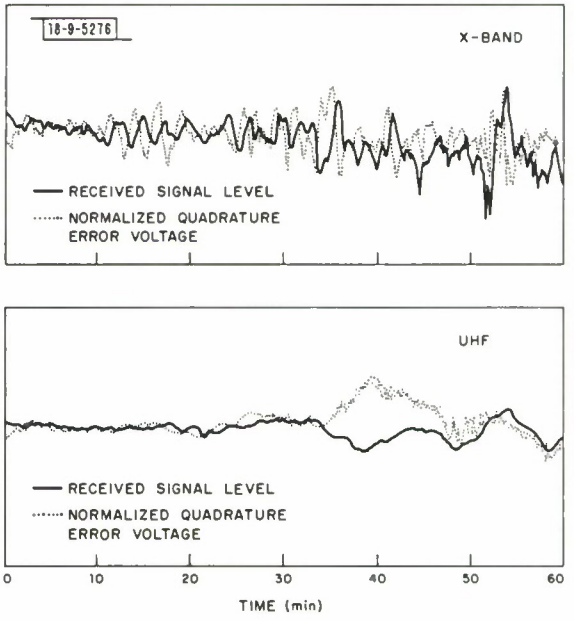

Fig. III-13. Comparison of received signal level and quadrature elevation angle error voltage fluctuations, low-angle data.

UHF, the antenna gain toward the horizon was less than 3 dB below the mainlobe peak at elevation angles below 1° which correspond to times between 15 and 60 min. Thus the most likely source of the multipath at UHF is ground reflection. The UHF elevation angle data displayed in Fig. III-10 were generated using only the nominal error voltage-to-angle calibration curve and hence the apparent fluctuations due to this multipath could be exaggerated.

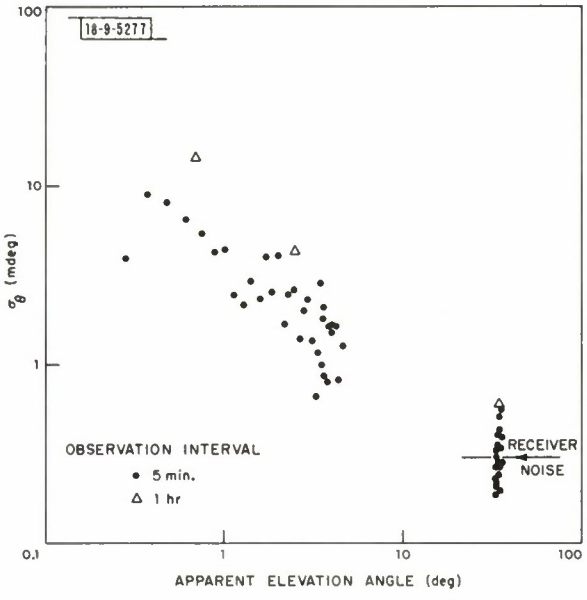

Fig. III-14. RMS fluctuations in elevation angle at X-band.

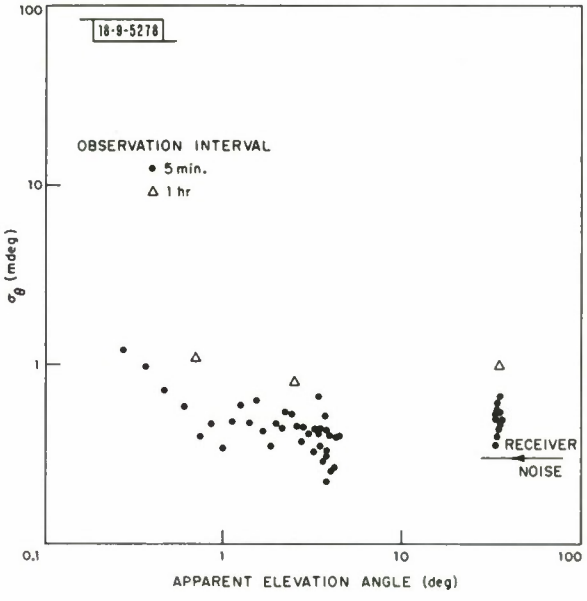

Fig. III-15. RMS fluctuations in traverse angle at X-band.

The 5-min. and 1-hr rms elevation angle fluctuations are given in Fig. III-14, and the corresponding rms traverse angle fluctuations are given in Fig. III-15. The traverse angle fluctuations are not significantly above the expected instrumental errors due to "glitches" and receiver noise at elevation angles above 0.5°. The elevation angle fluctuations are significantly greater than the instrumental noise at elevation angles below 10°. The 1-hr rms fluctuations in elevation angle are between 2 and 3 times the 5-min. values due to longer period (large-scale) fluctuations. The elevation angle fluctuations are roughly an order of magnitude larger than the traverse angle fluctuations at elevation angles below 1°.

C. Orthogonal Polarization Fluctuations

The orthogonal polarization signals were coherently detected at X-band and UHF using the principal polarization signal as reference. Quadrature video data with a 10-Hz bandwidth were recorded at both frequencies. The UHF quadrature video data were obtained only from July to the end of the year, and the 10-Hz predetection filters were only installed at Millstone prior to the November observations. The orthogonally polarized signal received at Millstone was roughly of the same level as the principally polarized signal, implying a linearly polarized signal at the source. At X-band, the orthogonal polarization signal ranged from 15 to 25 dB below the principal polarization signal. The variation in level was slow depending upon the satellite-to-ground station geometry and the particular satellite being observed. At high angles, the rms fluctuations in received power and in phase relative to the principal polarization signal were identical with the values expected for receiver noise.

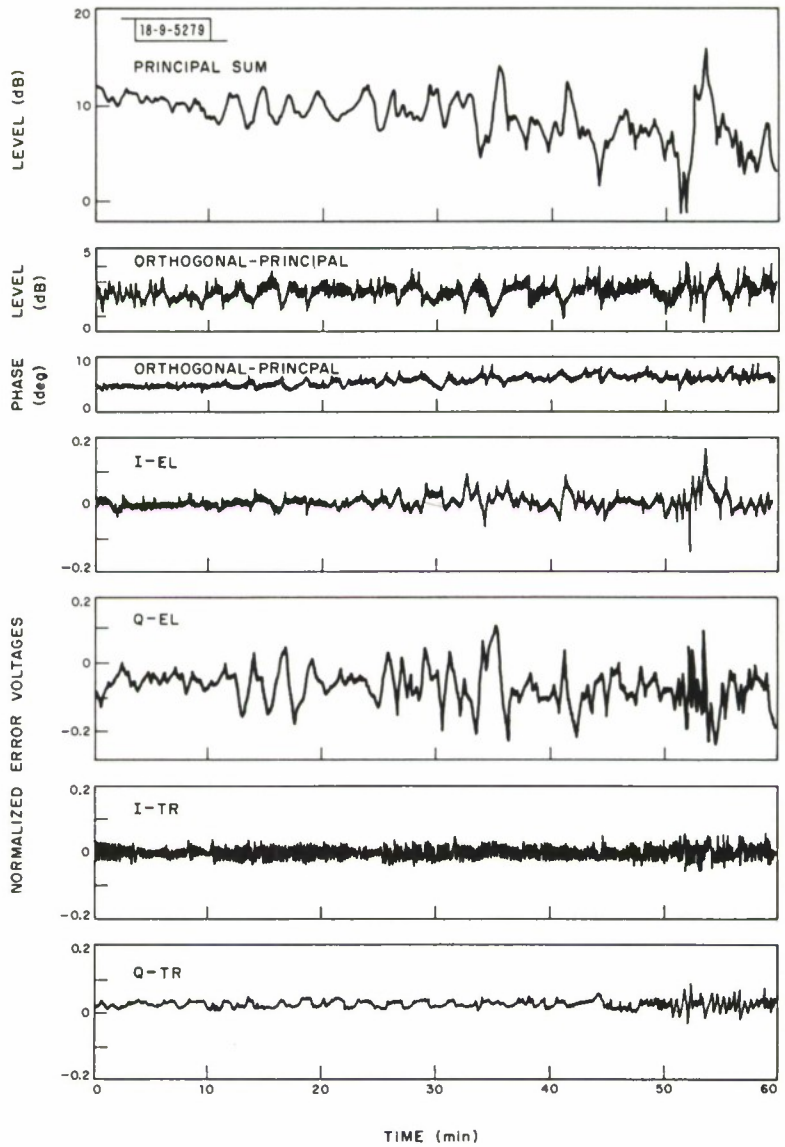

Fig. III-16. Received signal fluctuations in the principal and orthogonal polarization scan channels and the elevation and traverse difference channels, low-angle data at X-band.

The orthogonal polarization signal varied with respect to the principal polarization signal at low elevation angles as shown in Figs. III-16 and -17. Figure III-16 displays the logarithm and phase of the ratio of the orthogonal to principal polarization signals. Fluctuations in the ratio indicate differences in the propagation path at the two polarizations or variations due to the antenna. The complex error voltages are also displayed in the figure to help identify which ratio variations are due to antenna deviations and which variations are due to propagation. The large signal-level excursions at 52 min. are accompanied by ratio changes that appear to be due to angle-of-arrival deviations. On the other hand, the ratio variations during the multipath event that occurred between 10 and 20 min. are not correlated with angle-of-arrival deviations. These variations could, however, be caused by the cross-polarized antenna response to the different multipath components that combine to provide a composite signal which the antenna

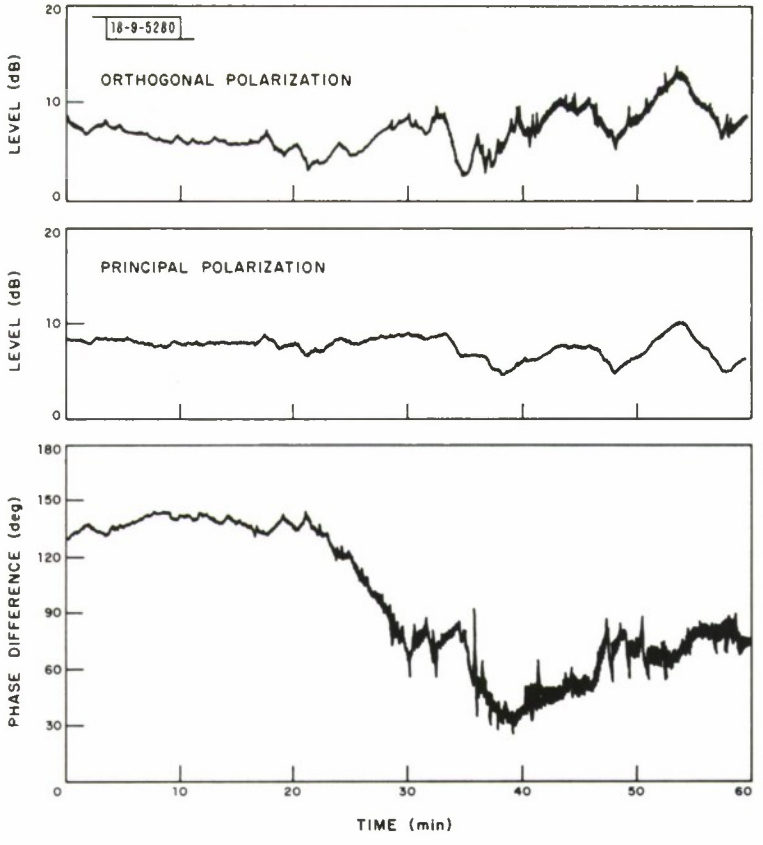

Fig. III-17. Received signal fluctuations in the principal and orthogonal polarization sum channels, low-angle data at UHF.

tracks. At UHF (Fig. III-17) the large phase variations observed, combined with larger differences between the logarithm of the orthogonal and principal power variations, are due to ground reflections.

IV. ANALYSIS

A. Statistical Summary

The fluctuation time histories depicted above are for two hours of observations at high, ~35°, and low, <1.5°, elevation angles. During the entire measurement series, 458 hours of observations were made on 37 days at different times of the day under different meteorological conditions. Roughly equal numbers of hours of observations were made during each season. The data all showed elevation-angle and signal-level fluctuations that were large at elevation angles near the horizon and decreased to very small values by 10° elevation angle. The data showed a slight seasonal dependence and a variation with time of day.

Observations of a single satellite rise or set provide a time history that is a single sample from a random process. An examination of a limited number of time histories is useful in obtaining a physical understanding of the fluctuation process. A quantitative measure of the process can only be acquired from the statistical moments of the process. These in turn are useful only if the process is stationary. The 5-min. and 1-hr rms fluctuation values depicted in Figs. IV-3, -4, -14, and -15 differed significantly suggesting that the process is not stationary. These problems will be examined in turn starting with a limited number of time-history examples.

A dependence of the magnitude of signal level and angle-of arrival fluctuations on elevation angle is evident from the time history of a satellite rise observed under clear sky conditions and displayed in Figs. IV-1 and -2. These data show large fluctuations in the X-band signal level, elevation angle, and quadrature component of the elevation angle error voltage at 1 to 2° elevation angles. The signal-level variations decrease from 11 dB peak-to-peak (p-p) at 2° El, to 3 dB p-p at 3° El, and 1.5 dB p-p at 5° El. The elevation angle variations do not decrease as rapidly, changing from 40 mdeg p-p at 2° El to 10 mdeg p-p at 5° El. The difference in the elevation angle dependences of signal level and elevation angle fluctuations is evident in the rms values plotted in Figs. IV-3 and -14. The elevation angle quadrature error voltage fluctuations appear to decay more rapidly with increasing elevation angle than do the signal level fluctuations. Significant quadrature error voltage variations occur only in combination with the quasi-periodic fluctuations typical of two-ray multipath. No significant error voltage fluctuations or signal level fluctuations are evident which correspond with the 10- to 20-mdeg pointing angle variations above 4°.

The data displayed in Figs. IV-1 and -2 can be interpreted as representing bias error fluctuations that depend only on the initial elevation angle (satellite-to-ground station) and not on time. If, as is usually assumed for ray-tracing analysis of bias errors due to refraction, the bias errors arise from the stratification of refractive index, the fluctuations due to the stratification should be identical for different azimuth directions.

L-band radar observations of the cross section of a calibration sphere are shown in Fig. IV-3. The observations were made toward the south then north and were separated in time by less than 16 min. The cross-section fluctuations represent signal level changes for the two-way path through the atmosphere, hence, are larger than the fluctuations for the one-way satellite beacon observations. For the 1-m^2 calibration sphere, LCS-4, the signal-to-noise ratio exceeded 30 dB for the 1-sec averages displayed in this figure. The error in measuring the rms log cross section resulting from receiver noise was less than 0.2 dB. The peak-to-peak cross-section variation between 2 and 3° elevation angle steering set exceeded 20 dB. The detailed fluctuation

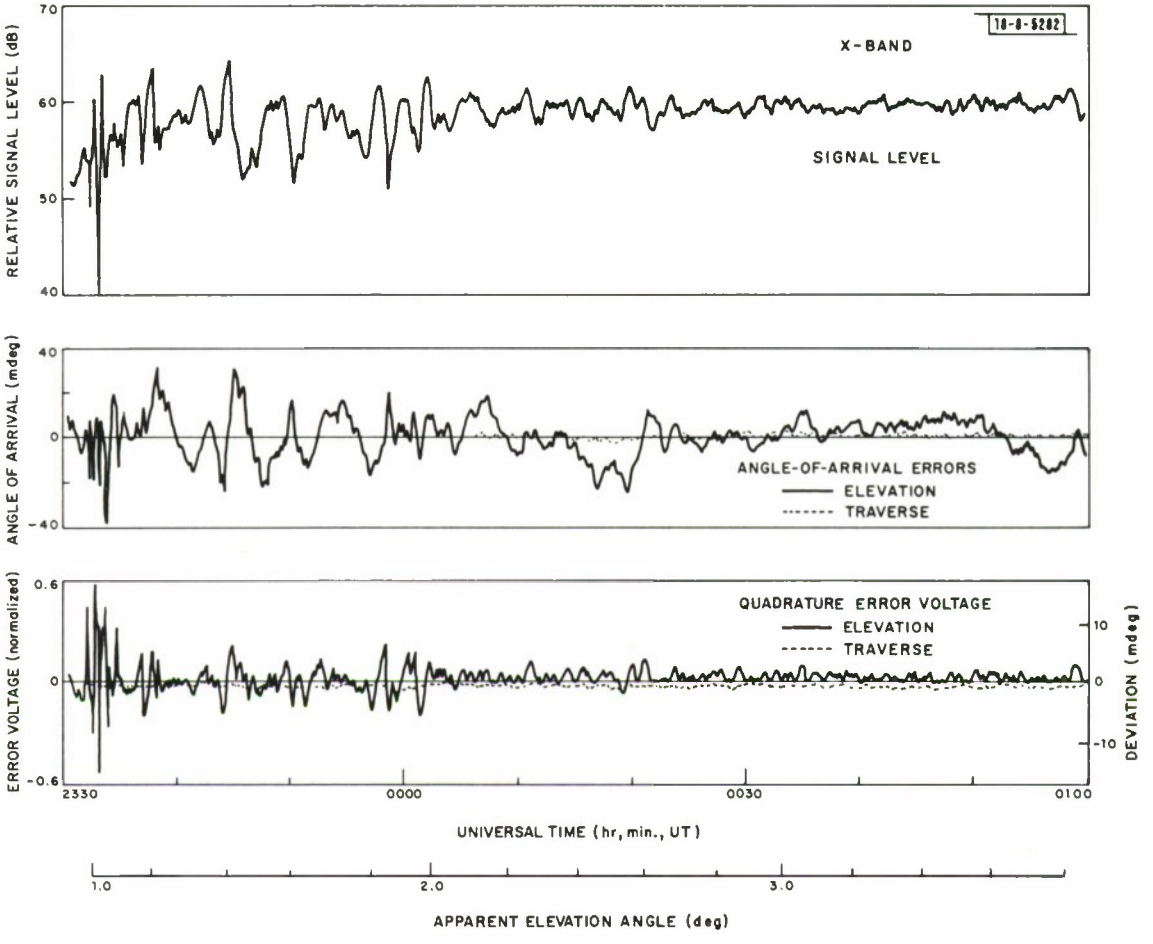

Fig. IV-1. Satellite rise, 2330 UT, 29 April 1975.

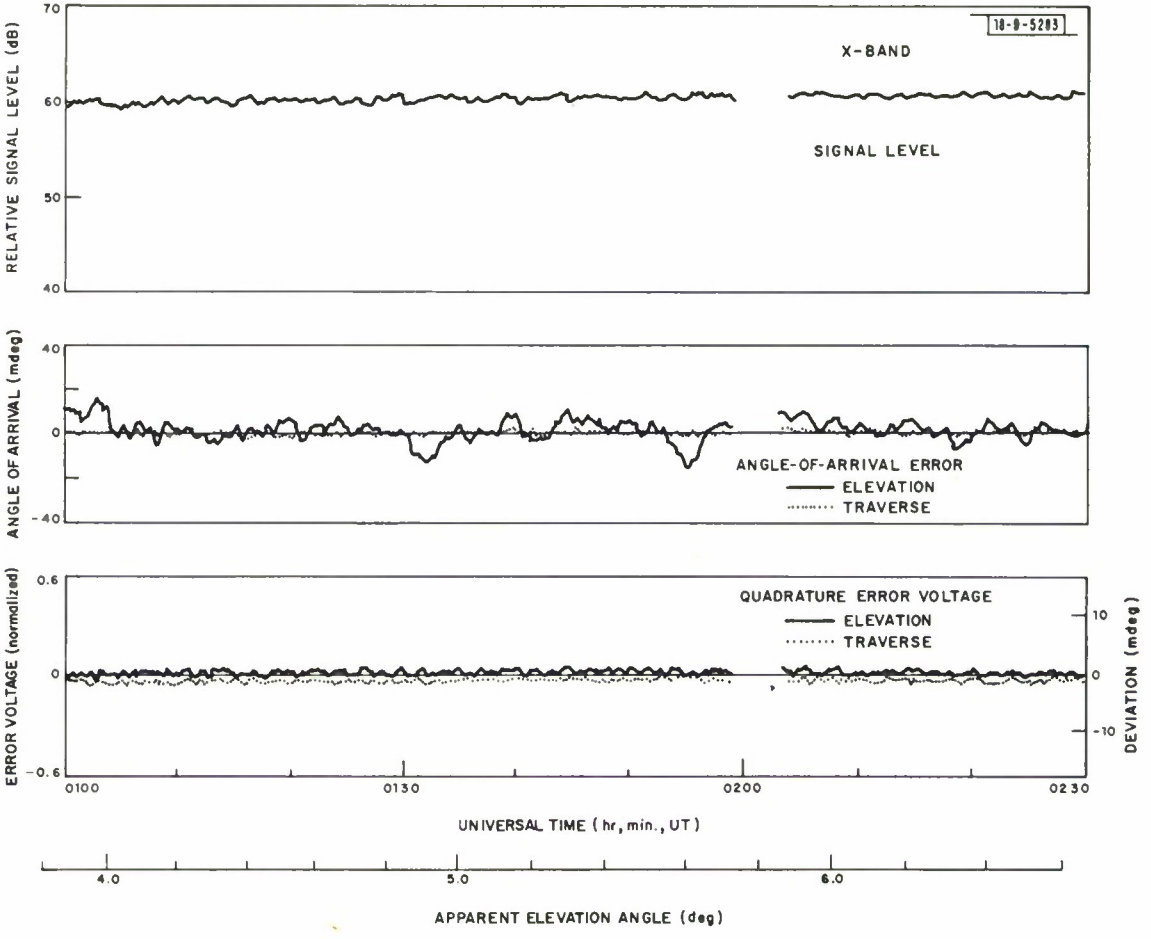

Fig. IV-2. Satellite rise continued, 0100 UT, 30 April 1975.

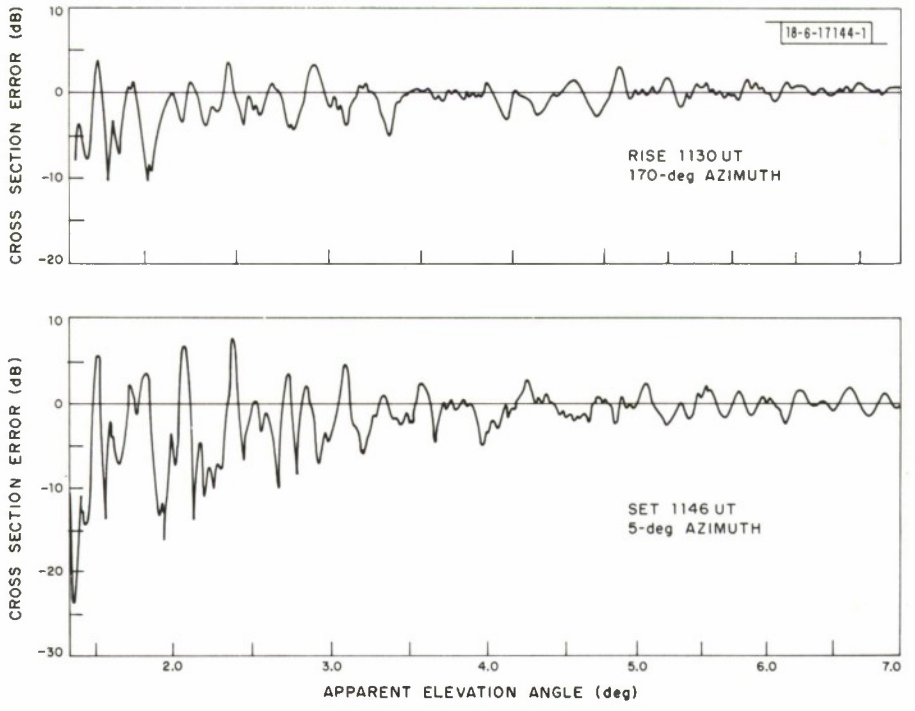

Fig. IV-3. L-band radar observations of a rise and set of a 1-m^2 calibration sphere (LCS-4, Object No. 5398).

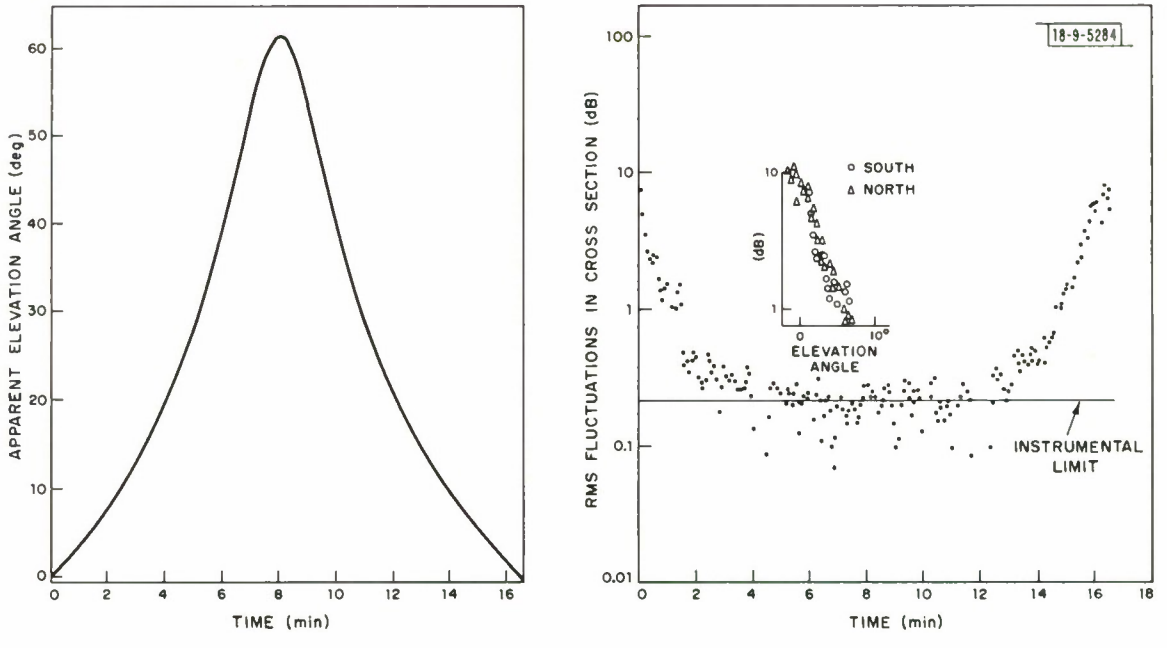

Fig. IV-4. Elevation angle and rms log cross section values for calibration sphere track depicted in Fig. IV-3.

time histories for observations to the north and south are different. Even the peak-to peak values differ. These data show that large-scale stratification alone is not responsible for the fluctuations. Figure IV-4 displays both the apparent elevation angle and rms cross section values for the same pass of LCS-4. The 0.2-dB noise limit is evident for elevation angles above 15°. The rms values in this plot were calculated for 8.5-sec intervals using the same detrending process as described above. Each 8.5-sec interval spanned less than 0.6° at elevation angles below 10° encompassing a sufficient number of fluctuations to provide a useful estimate of the variance of the process. The insert in Fig. IV-4 shows the rms values vs elevation angle and these are found to be identical toward the north and south. The rms values provide a good description of the fluctuation process because they are reasonably identical at the same elevation angles. Because the variance depends on elevation angle, larger observation intervals will have larger variances due to the change in elevation angle. Smaller observation intervals, however, would also produce a larger spread in the rms values due to a decrease in the number of fluctuations (samples) used in computing the value.

A time-of-day dependence in the fluctuations is also evident as shown in Fig. IV-5. These data are for three satellite rises observed six hours apart on the same day (same day as for

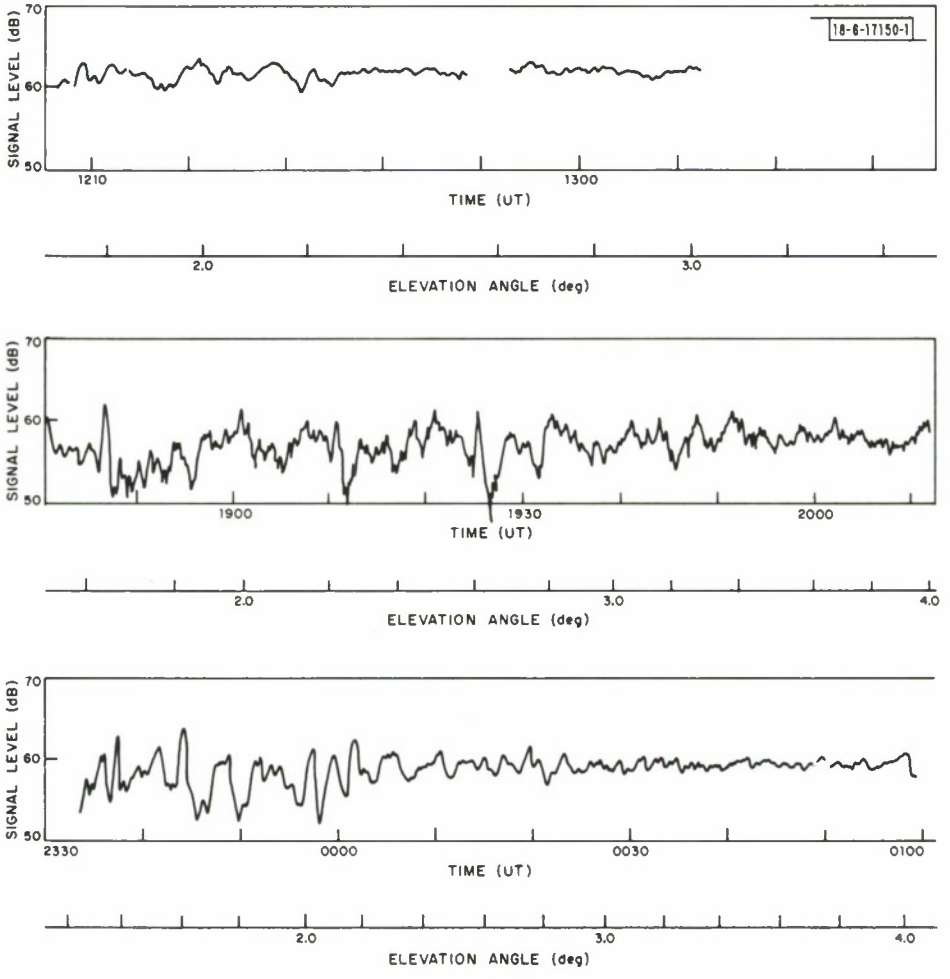

Fig. IV-5. Three satellite rises within 12 hours, 29 April 1975.

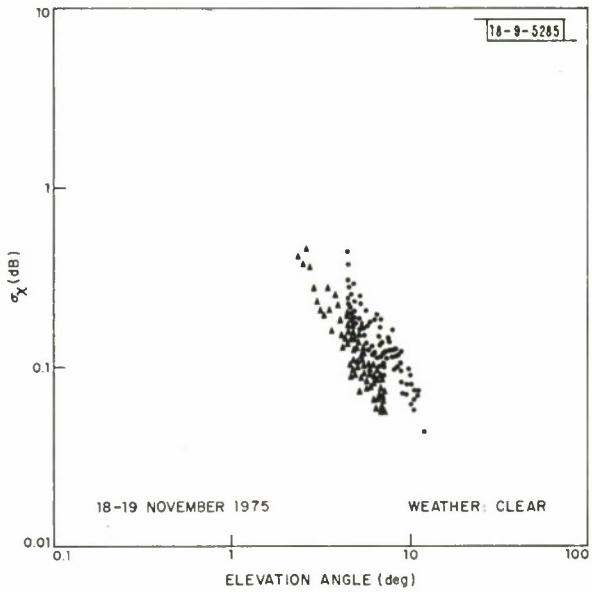

Fig. IV-6. RMS fluctuations in log power at X-band.

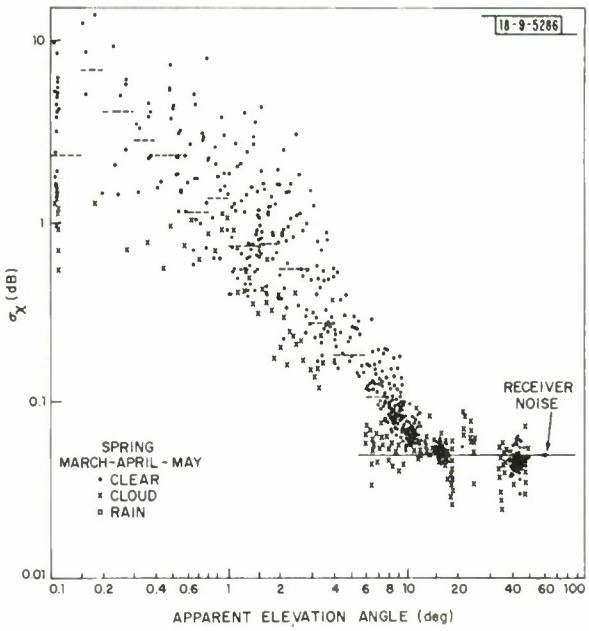

Fig. IV-7. RMS fluctuations in log power at X-band, spring season.

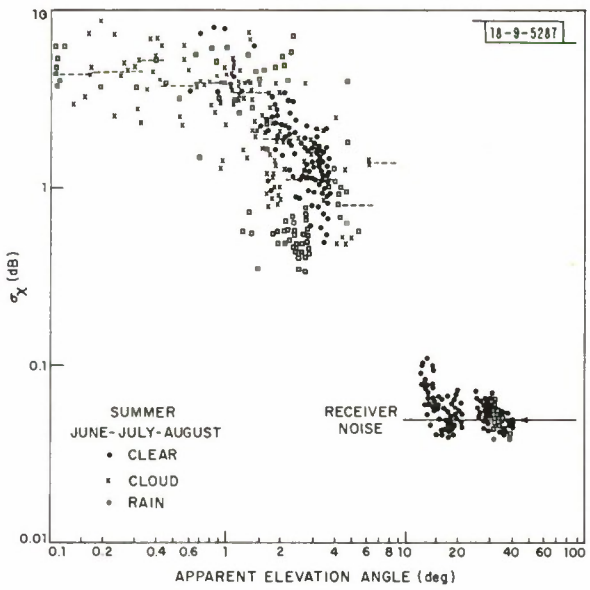

Fig. IV-8. RMS fluctuations in log power at X-band, summer season.

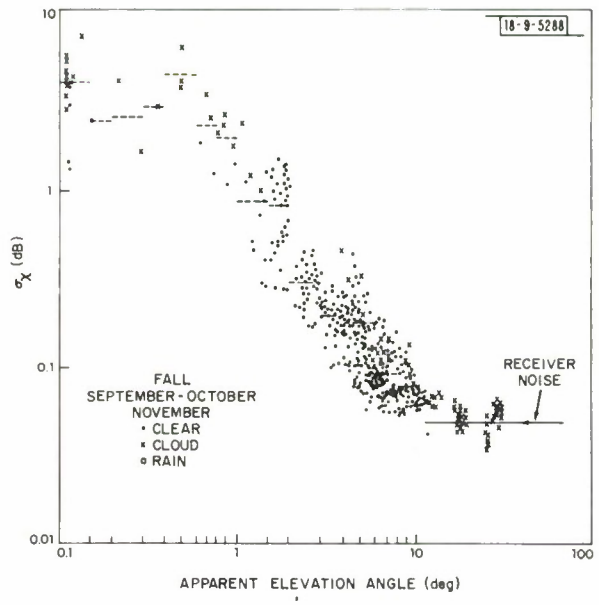

Fig. IV-9. RMS fluctuations in log power at X-band, fall season.

Figs. IV-1 and -2). The character of the fluctuations is markedly different for each rise. In the morning, low-frequency fluctuations with small peak-to-peak variations are evident. By afternoon, larger fluctuations are evident which have superimposed on them a high-frequency component. In the evening, the fluctuations remained large but the high-frequency component had disappeared. The rms variations at a given time of day span a relatively narrow dB range at a given elevation angle as shown in Fig. IV-4. The data displayed at elevation angles below 10° in Figs. IV-3, -4, -14, and -15 were all obtained within four hours. Although these data were obtained at azimuth angles near 100° and 260°, the spread in rms values at a given elevation angle is small. When the low elevation angle data are obtained from two sets of observations spaced by more than six hours, the data often fall into two different groups as shown in Fig. IV-6. Data for an entire season display a significant variation in rms values for a given elevation angle as shown in Figs. IV-7 through -14. Figures IV-15 and -16 summarize the extremes in the rms values for elevation angles between 1 and 10°.

The seasonal summaries encompass all the observations including days with clear skies, days with clouds (scattered fair-weather cumulus to complete overcast), and days with rain. Days with showery and widespread rain were encountered. A single observation set often encountered several weather types. Sets displayed as clear weather observations may have included thin scattered cirrus clouds. Data sets that encompassed clear sky and cloudy conditions were included in the "cloud" category. If rain occurred at any time within an observation set it was classified as "rain." No clear dependence on weather type was observed. In the spring the "cloud" data set showed lower fluctuations than for clear sky; in the fall the reverse occurred. In general, the summer data showed the largest fluctuations; the rest of the seasons were roughly the same. The elevation-angle fluctuations displayed a wider range of rms values than did the signal-level variations.

The 5-min. rms signal level variations ranged between 0.5 and 14 dB at elevation angles below 1°, and were less than 0.2 dB at elevation angles above 10°. No variations larger than the measurement error introduced by the receiver noise and satellite spin were evident at elevation angles above 15°. The 5-min. rms elevation angle fluctuations ranged between 1 and 100 mdeg for elevation angles below 1°. The summer values were significantly higher than for the other seasons at elevation angles below 1°. RMS values as high as 2 mdeg were observed at elevation angles as high as 30°. The clear-sky elevation angle fluctuation data were all below 1 mdeg rms for elevation angles above 10°. The elevation-angle fluctuations were measurable above the receiver noise for elevation angles up to 40°. The elevation-angle fluctuations are nearly identical to the predicted bias-error fluctuations expected using a surface correction model as shown in Fig. IV-16.

Fluctuations in traverse angle and in the ratio of the orthogonal-to-principal polarization signals are not discussed further because they did not show significant increases above instrument measurement noise at elevation angles above 1°.

B. Comparison with Scintillation Theory

Scintillation theory attempts to describe the random fluctuations in signal level and angle of arrival and relate the rms values to either the spectrum or correlation function describing the refractive index fluctuations along the ray path. At the present time, an adequate theoretical model exists only for weak scintillation when $\sigma_\chi < 5$ dB [(Ref. 9)]. The theory can be used to describe the dependence of the rms fluctuation values on frequency, propagation geometry, and on

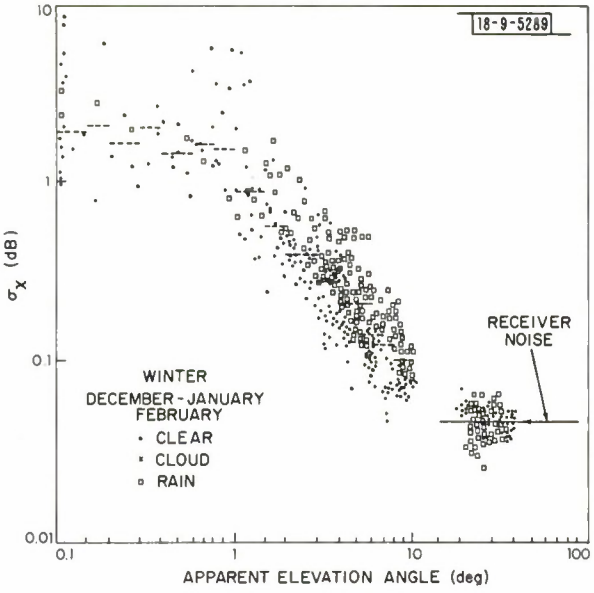

Fig. IV-10. RMS fluctuations in log power at X-band, winter season.

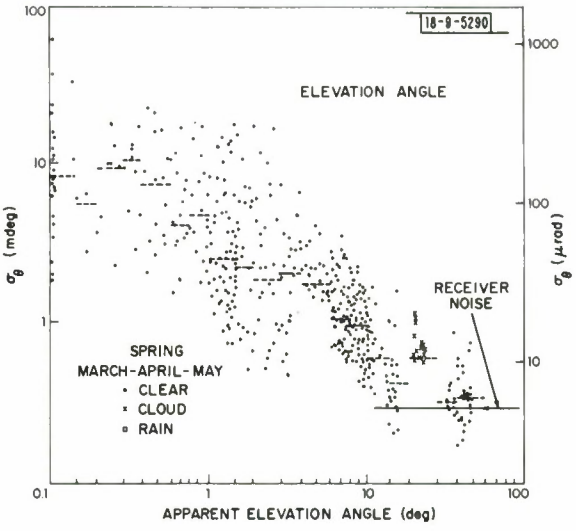

Fig. IV-11. RMS fluctuations in elevation angle at X-band, spring season.

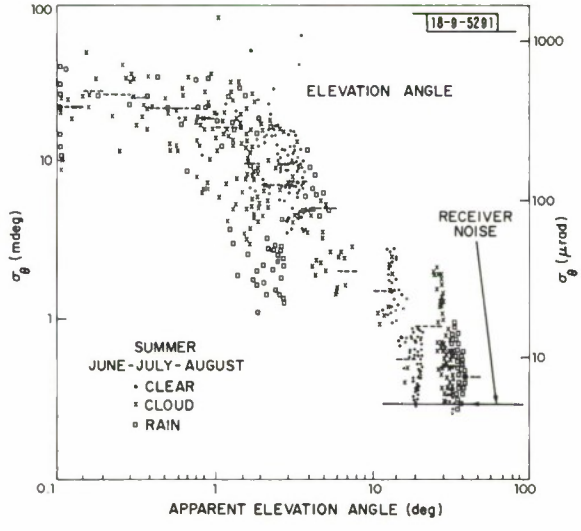

Fig. IV-12. RMS fluctuations in elevation angle at X-band, summer season.

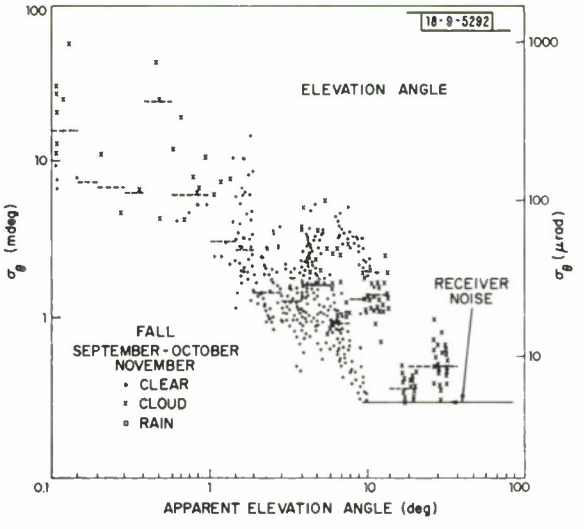

Fig. IV-13. RMS fluctuations in elevation angle at X-band, fall season.

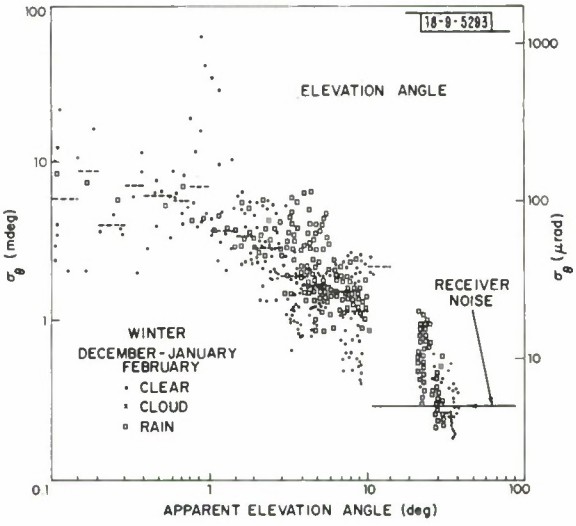

Fig. IV-14. RMS fluctuations in elevation angle at X-band, winter season.

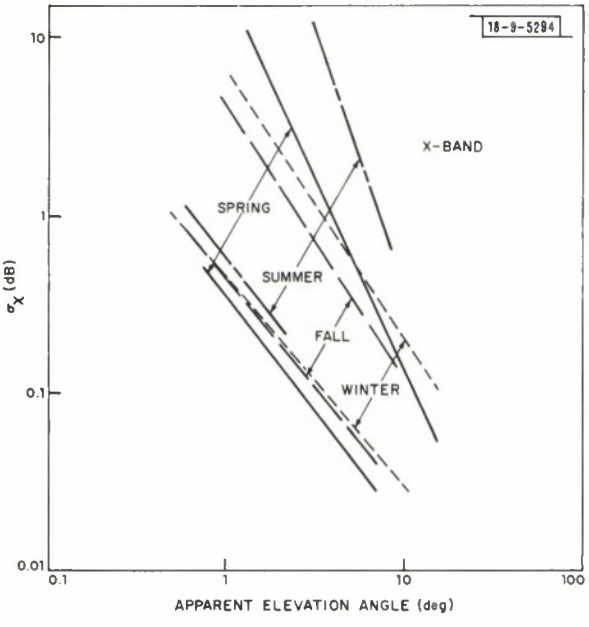

Fig. IV-15. RMS fluctuations in log power, full year.

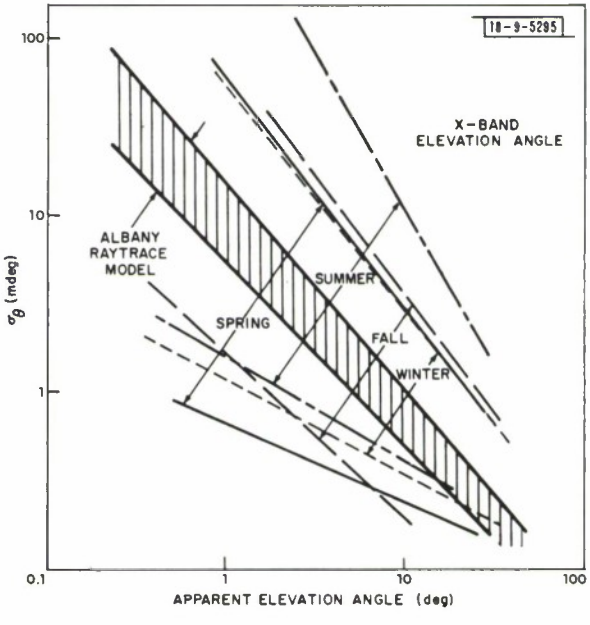

Fig. IV-16. RMS fluctuations in elevation angle, full year.

the intensity of either the turbulence or gravity (buoyancy) waves responsible for the refractive index fluctuations. Following Crane[8,9,10] and noting that the results for tropospheric scintillation can be obtained from the expressions developed for ionospheric scintillation by multiplication by $k^2/(2\pi r_e)$, then σ_χ in decibels becomes:

$$\sigma_\chi^2 = \left(\frac{40}{\ln 10}\right)^2 \frac{\Sigma_o^{p-3}\,\Gamma\left(\frac{p}{2}\right) b_p}{\Gamma\left(\frac{3}{2}\right)\Gamma\left(\frac{p-3}{2}\right) 2^{p/2} k^{(p-2)/2}} \int_{\ell_1}^{\ell_2} I_p G(\alpha,\psi)\,\sigma_N^2(\rho)\, Z^{(p-2)/2}\, d\rho \qquad (1)$$

where

$\Sigma_o = 2\pi/Lo$, Lo = outer scale of turbulence (or gravity waves)

p = exponent of power spectrum of refractive index fluctuations $\Phi_N(\underset{\sim}{\kappa})$

α = axial ratio for the refractive index spectrum

ψ = zenith angle of tangent to ray at p

$k = 2\pi/\lambda$, λ = wavelength

r_e = classical electron radius[9]

σ_N^2 = variance of the refractive index fluctuations

$Z = \rho(L-\rho)/L$, L = length of ray path, ρ = position along ray

$$b_p \begin{cases} = -\Gamma\left(\frac{2-p}{2}\right)\cos\left(\frac{p-2}{4}\,\pi\right) 2^{(p-4)/2} & ; \quad 2 < p < 6 \quad ; \quad p/4 \\ = \pi/2 & ; \quad p = 4 \end{cases}$$

$$I_p \begin{cases} = \frac{1}{2\pi}\int_0^{2\pi} [(\cos^2\psi + \alpha^2 \sin^2\psi)\cos^2\theta + \sin^2\theta]^{(p-2)/2}\, d\theta \\ = 1 & ; \quad \alpha = 1 \end{cases}$$

$$G(\alpha,\psi) = \frac{\alpha}{2}\,\frac{(1 + \cos^2\psi + \alpha^2\sin^2\psi)}{(\cos^2\psi + \alpha^2\sin^2\psi)^{(p-1)/2}}$$

and the power spectrum for refractive index fluctuations is given by:

$$\Phi_N(p, \underset{\sim}{\kappa}) = \frac{\sigma_N^2(\rho)\,\alpha L_o^3\,\Gamma(p/2)}{2\pi\Gamma(3/2)\,\Gamma\left(\frac{p-3}{2}\right)\left[1 + \left(\frac{L_o}{2\pi}\right)^2 (\kappa_h^2 + \alpha^2\kappa_v^2)\right]^{p/2}}$$

κ = wavenumber = $2\pi/d$, d = scale size

κ_h, κ_v = horizontal and vertical wavenumbers.

For isotropic turbulence ($\alpha = 1$) with $p = 11/3$ and L_o and L very large, this expression can be reduced to the equation given by Tatarski[15]

$$\sigma_\chi^2 = \left(\frac{20}{\ln 10}\right)^2 0.56k^{7/6} \int_o^L C_N^2(\rho)\, p^{5/6}\, d\rho \qquad (2)$$

where C_N^2 replaces σ_N^2 as a measure of the intensity of turbulence.

A reasonable expression for the angle-of-arrival variance requires a better understanding of the values to be used in describing the power spectrum for the refractive-index fluctuations. For ionospheric scintillation, L_o exceeds any scale size associated with atmospheric drift across the path during a measurement interval.[10] In that case, a reasonably simple approximate expression for σ_θ^2 can be generated. From analyses of tropospheric scintillation data reported by Tatarski,[15] it is evident that L_o is larger than the Fresnel zone sizes typical of microwave and optical propagation through the lower atmosphere. For tropospheric turbulence at scale sizes smaller than L_o, the spectrum is isotropic.[16] Anisotropy ($\alpha < 1$) occurs at scale sizes larger than L_o. Since, for the Haystack measures, the elevation-angle fluctuations greatly exceed the traverse-angle fluctuations, L_o must be smaller than the scale sizes associated with atmospheric drift by the line of sight and a 5-min. observation period. For a nominal 10-m/sec drift by the line of sight, $L_o << 3$ km.

The expressions for σ_χ given in Eq. (1) and (2) were derived using the Rytov approximation and are only valid for weak scintillation.[9] The X-band and UHF observations were used to check the weak-scintillation frequency dependence given by Eq. (2). Five-minute σ_χ observations made simultaneously at both frequencies are plotted in Fig. IV-17. Two curves separated by

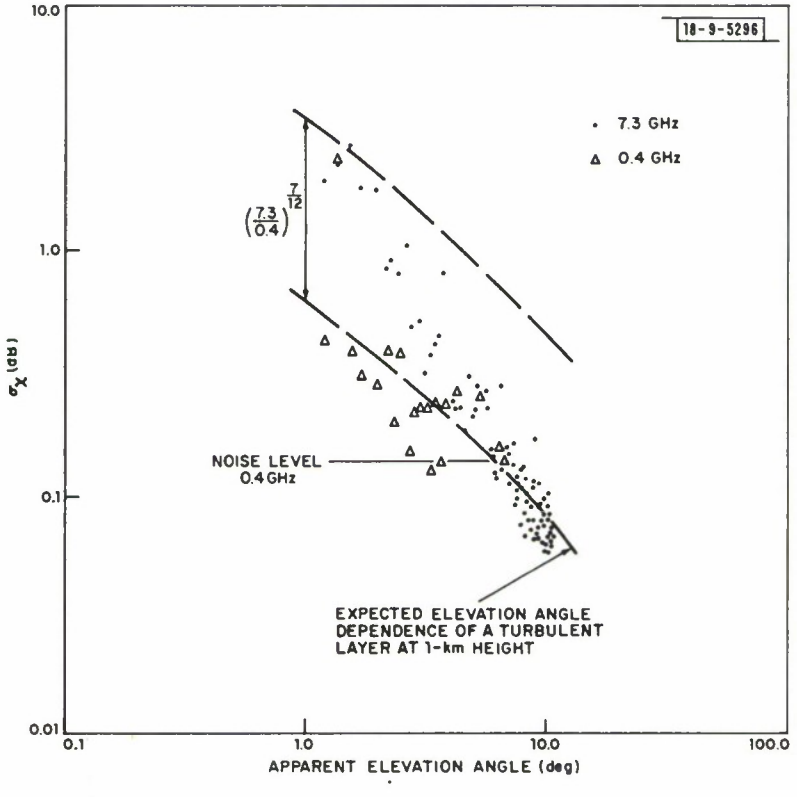

Fig. IV-17. RMS fluctuations in log power at X-band and UHF, 29-30 April 1975.

$\lambda^{-7/12}$ were plotted on this figure to represent the expected frequency dependence. These curves were generated for a hypothetical turbulent layer at a 1 km height. The UHF data can be interpreted as being in reasonable agreement with this expected elevation-angle dependence. The X-band data are not in agreement and exhibit a significant decrease in σ_χ as the elevation angle increases. This discrepancy may be due in part to a reduction in the X-band fluctuations caused by averaging over the 36.6-m antenna aperture. This latter effect was discussed by Tatarski.[13] He showed that the rms fluctuations are reduced by 20 percent for a uniformly weighted circular aperture when the diameter is one-half of the size of the first Fresnel zone $\sqrt{\lambda Z}$. The distance between the layer and the antenna rapidly decreases below the value required for the first Fresnel zone size to equal the diameter of the aperture as the elevation angle increases producing the apparently steeper slope for the X-band data. The angle-of-arrival fluctuations are dominated by the large scale sizes, $d >> \sqrt{\lambda Z}$, which are not severely attenuated by aperture averaging. As a result, the elevation angle-of-arrival data have an elevation angle dependence similar to that for the UHF data (see Figs. IV-3, -4, and -14).

The weak scintillation theory model is not valid when the signal-level fluctuations become large.[9] For large fluctuations or strong scintillation, the time histories reveal a number of randomly occurring multipath events. These events appear to be characteristic of strong scintillation. Currently, a viable strong scintillation model is not available.

The weak-scintillation results given above were derived using a power spectrum for the refractive index perturbations that is often observed for atmospheric turbulence.[14] The behavior of the spectrum at the larger scale sizes of importance to angle-of-arrival fluctuations is not known. The theoretical analysis used to derive Eq. (1) only assumed the existence of a spectrum and its general shape, but not its cause. The fluctuations could be due to gravity waves or to turbulence. Although a distinction is usually drawn between waves and turbulence, for scintillation the differences between the two phenomena are not important; the shape of the spectrum, however, is of importance.

The angle-of-arrival fluctuations are dominated by the large scale size refractive index perturbations. At large scale sizes, the propagation phenomena are adequately described by geometrical optics (ray tracing). In the limit of geometrical optics (the Rytov approximation at large scale sizes), the angle-of-arrival fluctuations are independent of frequency. At high frequencies, the signal-level fluctuations, σ_χ, increase as $f^{7/12}$ (as $\lambda^{-7/12}$). For a fixed aperture size, σ_χ, however, decreases due to the increase in $D/\sqrt{\lambda Z}$ where D is aperture diameter. Again for a fixed aperture size, the elevation-angle fluctuations increase as a *percentage* of the beamwidth as the frequency increases (increase is linear with frequency).

V. CONCLUSIONS

Observations of tropospheric scintillation were made at Haystack and Millstone. Elevation-angle fluctuations were evident above the instrumental measurement noise at initial elevation angles ranging from the horizon to 43°. The median values for the rms fluctuations within a 5-min. observation period are displayed in Fig. V-1 for each season. These data represent the elevation angle measurement uncertainties expected during a 5-min. observation period due to the troposphere. Single-antenna radar systems will not achieve better measurement accuracies. This result is independent of frequency. The expected rms residuals for bias error estimation calculated using the surface refractive correction model are nearly the same magnitude as these

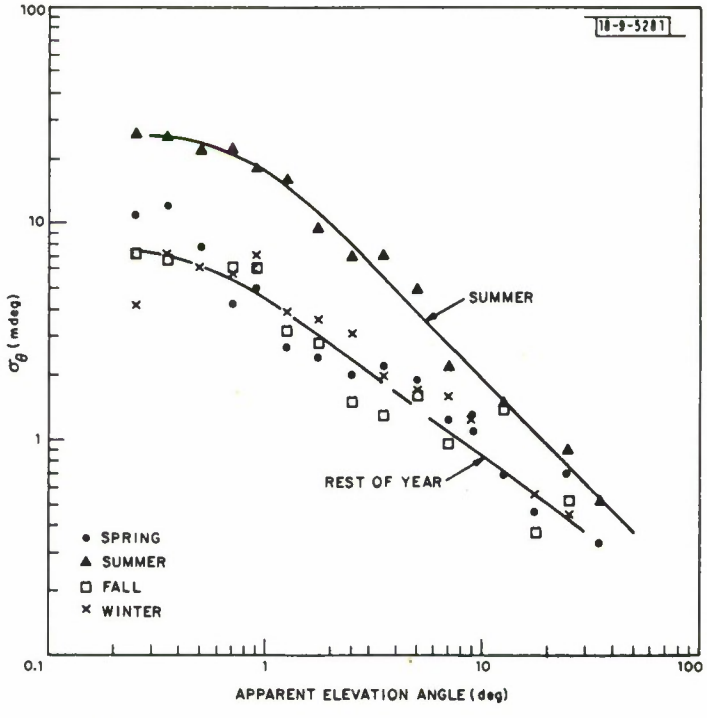

Fig. V-1. Median rms fluctuations in elevation angle by season.

values. Because refraction correction estimates apply for time intervals longer than five minutes, the median rms values displayed in Fig. V-1 represent the minimum errors in providing for bias refraction. Since the surface correction model provides estimates with errors comparable to the minimum possible, it provides a reasonable correction procedure. More elaborate procedures designed to provide a better estimate of the bias errors at one instant of time are therefore not warranted.

The tropospheric scintillation observations were in qualitative agreement with the predictions of weak scintillation theory for elevation angles above 2 to 3°. The signal-level fluctuation data show severe aperture averaging using the Haystack 36.6-m antenna. The aperture averaging did not significantly affect the angle-of-arrival scintillation. At elevation angles below 2 to 3°, strong scintillation occurred. The strong scintillation was a result of a number of randomly occurring multipath events. During the strong scintillation multipath events, signal depolarization was noted. The change in apparent polarization is presumed to be caused by the response of the antenna to the multiple signals received at slightly differing angles of arrival.

REFERENCES

1. J. V. Evans, editor, "Millstone Hill Radar Propagation Study: Scientific Results, Parts I, II, and III," Technical Report 509, Lincoln Laboratory, M.I.T. (13 November 1973), DDC Nos.: Part I, AD-781179/7; Part II, AD-782748/8; Part III, AD-780519/5.
2. D. K. Barton, Chapter 15 in Radar System Analysis (Prentice Hall, Englewood Cliffs, N. J., 1964).
3. B. R. Bean, E. J. Dutton, and B. D. Warner, Chapter 24, "Weather Effects on Radar," in Radar Handbook, M. I. Skolnik, editor (McGraw-Hill, New York, 1970).
4. R. K. Crane, Sec. 2.5, "Refraction Effects in the Neutral Atmosphere," in Methods of Experimental Physics, Vol. 13B, M. L. Meeks, editor (Academic Press, New York, 1976).
5. J. V. Evans, editor, "Millstone Hill Radar Propagation Study," Technical Note 1969-51, Lincoln Laboratory, M.I.T. (26 September 1969), DDC AD-701939.
6. J. C. Ghiloni, editor, "Millstone Hill Radar Propagation Study: Instrumentation," Technical Report 507, Lincoln Laboratory, M.I.T. (20 September 1973), DDC AD-775140/7.
7. J. V. Evans, editor, "Millstone Hill Radar Propagation Study: Calibration, "Technical Report 508, Lincoln Laboratory, M.I.T. (3 October 1973, DDC AD-779689/9.
8. R. K. Crane, "Spectra of Ionospheric Scintillation, J. Geophys. Res. 81, 2041 (1976).
9. R. K. Crane, "Ionospheric Scintillation," Proc. IEEE (accepted for publication, 1977).
10. R. K. Crane, "Variance and Spectra of Angle-of-Arrival and Doppler Fluctuations Caused by Ionospheric Scintillation," J. Geophys. Res. (submitted for publication, 1976).
11. R. K. Crane, "Propagation Phenomena Affecting Satellite Communication Systems Operating in the Centimeter and Millimeter Wavelength Bands," Proc. IEEE 59, 173 (1971), DDC AD-728187.
12. M. L. Meeks and J. Ruze, "Evaluation of the Haystack Antenna and Radome," IEEE Trans. Antennas and Propag. AP-19, 723 (1971), DDC AD-737166.
13. H. G. Weiss, "The Haystack Microwave Research Facility," IEEE Spectrum 2, No. 2, 50 (1965), DDC AD-614734.
14. S. M. Sherman, "Complex Indicated Angles Applied to Unresolved Radar Targets and Multipath," IEEE Trans. Aerospace Electron. Systems AES-7, 160 (1971).
15. V. I. Tatarskii, The Effects of the Turbulent Atmosphere on Wave Propagation (Nauka, Moscow, 1967). (Translation available U. S. Department of Commerce, National Technical Information Service, Springhill, Virginia, 1971.)
16. A. S. Monin and Y. M. Yaglom, Statistical Fluid Mechanics, Vol. 2 (M.I.T. Press, Cambridge, Mass., 1975).

REPORT DOCUMENTATION PAGE		READ INSTRUCTIONS BEFORE COMPLETING FORM
1. REPORT NUMBER ESD-TR-76-115	2. GOVT ACCESSION NO.	3. RECIPIENT'S CATALOG NUMBER
4. TITLE *(and Subtitle)* Low Elevation Angle Measurement Limitations Imposed by the Troposphere: An Analysis of Scintillation Observations Made at Haystack and Millstone		5. TYPE OF REPORT & PERIOD COVERED Technical Report 6. PERFORMING ORG. REPORT NUMBER Technical Report 518
7. AUTHOR*(s)* Robert K. Crane		8. CONTRACT OR GRANT NUMBER*(s)* F19628-76-C-0002
9. PERFORMING ORGANIZATION NAME AND ADDRESS Lincoln Laboratory, M.I.T. P.O. Box 73 Lexington, MA 02173		10. PROGRAM ELEMENT, PROJECT, TASK AREA & WORK UNIT NUMBERS 8X363304D215
11. CONTROLLING OFFICE NAME AND ADDRESS Ballistic Missile Defense Program Office Department of the Army 1320 Wilson Boulevard Arlington, VA 22209		12. REPORT DATE 18 May 1976 13. NUMBER OF PAGES 40
14. MONITORING AGENCY NAME & ADDRESS *(if different from Controlling Office)* Electronic Systems Division Hanscom AFB Bedford, MA 01731		15. SECURITY CLASS. *(of this report)* Unclassified 15a. DECLASSIFICATION DOWNGRADING SCHEDULE

16. DISTRIBUTION STATEMENT *(of this Report)*

Approved for public release; distribution unlimited.

17. DISTRIBUTION STATEMENT *(of the abstract entered in Block 20, if different from Report)*

18. SUPPLEMENTARY NOTES

None

19. KEY WORDS *(Continue on reverse side if necessary and identify by block number)*

index of refraction	X-band	bias errors	Haystack radar
tropospheric propagation	UHF	Millstone radar	IDCSP satellites
amplitude scintillation	multipath		

20. ABSTRACT *(Continue on reverse side if necessary and identify by block number)*

Tropospheric angle-of-arrival and amplitude scintillation measurements were made at X-band (7.3 GHz) and at UHF (0.4 GHz). The measurements were made using sources on satellites with 12-day orbits. The angle of arrival of the ray path to a satellite changed slowly allowing observations of fluctuations caused by atmospheric irregularities as they slowly drifted across the ray path. The fluctuations were characterized by the rms variations of elevation angle and the logarithm of received power (log power).

Over a one-year period, 458 hours of observation were amassed spanning every season, time of day, and weather conditions. The results show strong scintillation occurrences below

20. ABSTRACT *(Continued)*

1 to 2° elevation angles characterized by a number of random occurrences of multipath events that produce deep fades, angle-of-arrival fluctuations, and depolarization of the received signal. The log power fluctuations ranged from 1 to 10 dB rms at elevation angles below 2° to less than 0.1 dB at elevation angles above 10°. The elevation angle fluctuations ranged from 1 to 100 mdeg at elevation angles below 2° to less than 5 mdeg at a 10° elevation angle. Comparable fluctuations in elevation angle are expected for bias refraction correction models based upon the use of surface values of the refractive index.